Validation and investigation of large-scale neural recordings across multiple visual brain areas of mice

A Dissertation
Presented to
The Academic Faculty

by

Donghoon Shin

In Partial Fulfillment
of the Requirements for the Degree
Master in Science in the
Electrical and Computer Engineering Department

Georgia Institute of Technology
December, 2020

Validation and Investigation of large-scale neural recordings across multiple visual brain areas of mice

Approved by:

Dr. Bilal Haider, Advisor
School of Biomedical Engineering
Georgia Institute of Technology

Dr. Christopher Rozell, Co-advisor
School of Electrical and Computer Engineering
Georgia Institute of Technology

Dr. Robert Liu
School of Biomedical Engineering
Emory University / Georgia Institute of Technology

Date Approved: December 4, 2020

ACKNOWLEDGEMENTS

I would like to thank Bilal for not just valuable advice and mentoring but also for emotional support and for serving as a role model. I thank Chris for the feedback and advice on the tracking algorithm in easy words that I could understand and Robert for giving me advice on the thesis. I also thank Armel for leading the ISI project and for helping me settle into the lab; and Kayla and Anderson for answering all my questions, and for giving me advice and feedback. I would like to thank all the other Haider lab members for answering my many questions, giving advice, and being all around good friends.

And finally, I thank my family for unconditioned and unlimited love and support, and Hyeri, Jeonghoon, Shea, Austin, Will, Wookjin and Suin for being with me during unprecedented COVID-19 times. I thank Mike and Kayla for proofreading this thesis.

.

CONTENTS

LIST OF TABLES

LIST OF FIGURES

LIST OF SYMBOLS AND ABBREVIATIONS

V1	Primary visual cortex
HVA	Higher visual areas of cortex
LGN	Lateral geniculate nucleus
LFP	Local Field Potential
CSD	Current source density
TLFC	Time-lagged functional connectivity
TSFC	Time-synced functional connectivity
RF	Receptive field
ISI	Intrinsic signal imaging
BOLD	Blood-oxygen-level-dependent
VFS	Visual field sign
NBG	Narrowband gamma oscillation
BBG	Broadband gamma oscillation
STLFP	Spike-triggered LFP

SUMMARY

The recently developed ability to simultaneously record thousands of neurons provides unprecedented opportunity for answering important questions about the brain. However, reliable analysis of large-scale neural data has to be established in advance to answer questions. The conducted project is two-fold: In the first half, I validated the reliability of large-scale neural data analysis, and in the second half, I applied these methods to large-scale neural data to investigate how neural information processing in mice is influenced by neural oscillations in multiple visual brain areas.

To validate the method, I first benchmarked two commonly used spike-sorting algorithms: Kilosort2 and Klustakwik2 in detectability of pairwise neuronal functional connectivity. Then, I developed an analysis pipeline of intrinsic signal imaging that non-invasively identifies specific visual cortical areas and their functional map.

Then, I applied these validated methods to investigate coherent narrowband gamma oscillations (NBG) close to 60Hz (50 -70Hz) and prominent in multiple visual areas of mice during visual processing. More specifically, I investigated how NBG is represented in visual areas and inspect the role of NBG in visual processing.

NBG is present in higher visual areas (HVAs) as well as in the visual thalamus and the primary visual cortex, as previously detailed in literature. Interestingly, there is a hierarchy of the coherence and power of NBG present in HVAs and it is consistent with the thalamo-cortical hierarchy that processes visual stimuli. Also, narrowband gamma propagates through local subnetworks rather than globally. Moreover, two neuronal

clusters exist in LGN and exhibit two different coherent NBGs, and also have different visual preference to ON/OFF stimulus.

With this result, I suggest two hypotheses for the role of NBG: First, that NBG synchronize visual brain areas for efficient communication between them, also known as the "communication through coherence" hypothesis. Second, that narrowband gamma encodes luminance information in a computationally efficient way.

CHAPTER 1. INTRODUCTION

1.1 The problem

The objective of the proposed research is two-fold: first, to validate the reliability of large-scale neural data analysis, and second, to apply reliable methods to large-scale neural data to investigate how neural oscillations in multiple visual brain areas of mice influence neural information processing.

The development of the Neuropixels probe has enabled electrical recording of neural activity from thousands of neurons in multiple visual areas simultaneously. (Jun et al., 2017) With this unprecedented opportunity, it is possible to investigate neural information processing in multiple visual areas simultaneously. Specifically, I am interested in how previously found coherent gamma oscillations prominent in multiple visual areas of mice affect visual sensory processing. (Niell and Stryker, 2010; Saleem et al., 2017; Storchi et al., 2017) I asked three questions about the neural oscillation:

1. Does coherent gamma oscillation previously found in visual thalamus (LGN) and primary visual cortex (V1) exist in higher visual areas?
2. How does neural oscillation propagate between multiple visual areas?
3. What is the role of this gamma oscillation in multiple visual areas?

However, reliable analysis of large-scale neural data must be established in advance to answer these questions. There are two main factors that prevent the reliable analysis of large-scale electrophysiology recordings (Steinmetz et al., 2018):

1. The deficit of ground truth dataset and variability between spike-sorting algorithms.

2. Variability in location of probe insertion sites.

To cope with these problems suggested by (Steinmetz et al., 2018), I first benchmarked two commonly used spike-sorting algorithms with the metric of single unit stimulus response properties and the statistical likelihood of detecting short-latency interactions between pairs of simultaneously recorded neurons. Also, I developed a post-processing pipeline of a non-invasive brain imaging system that reveals visuo-cortical areas before inserting probes.

1.2 Introduction

The recent development of the Neuropixels probe (Jun et al., 2017) enables electrophysiological recording from thousands of neurons simultaneously. However, isolating action potentials (spikes) from single neurons (spike-sorting) is still an unresolved problem that not only requires significant computation but also lacks ground truth. In addition, spike-sorting shows large variability between algorithms. (Magland et al., 2020; Steinmetz et al., 2018)

Multiple studies have compared the performance of spike-sorting algorithms. From these papers it is known that different spike-sorting algorithms give different results in miss rates and false-positive rates using hybrid ground-truth datasets. (Alessio P. Buccino, 2019; Magland et al., 2020) However, there remain many questions regarding the constraints posed by different spike-sorting algorithms, and how these may interact with other

experimental conditions such as choice of probes, analysis methods, areas of the brain, and visual stimuli.

First, I compared the performance and constraints posed by two commonly used spike-sorting algorithms: 1) Klustakwik2, (Rossant et al., 2016) the algorithm that the Haider lab has used extensively for 32- 64 channel Neuronexus probes (Speed et al., 2019; Speed et al., 2020; Williams et al., 2020), and 2) Kilosort2, the algorithm that the lab plans on using primarily for Neuropixels with 384 channels. (Pachitariu et al., 2016b) The analysis focused specifically on neural activity evoked by visual stimulation of receptive fields (RF) in primary visual cortex (V1) of awake mice and also during a visual stimulus detection task. I used analysis methods that have been used previously (Speed et al., 2019; Speed et al., 2020; Williams et al., 2020) to analyze neural data to quantify the different effect of two spike-sorting algorithms on single unit stimulus response properties, as well as on the statistical likelihood of detecting pairwise short-latency interactions between pairs of simultaneously recorded neurons.

Second, identifying the specific brain area of interest non-invasively before inserting an invasive electrical probe presents several challenges. These challenges include the small size of the mouse brain, mouse to mouse variability in the region of interest, and the existence of the skull, which filters and attenuates brain signals.

The development of the Allen Mouse Brain Common Coordinate Framework (Allen CCF) provides a unified coordinate system for mapping brain areas repeatedly between labs in targeting mouse brain areas. (Wang et al., 2020) However, Allen CCF

ignores mouse to mouse variability in the brain anatomy which requires a technique that reveals anatomy of each specific mouse.

In studying rodent sensory systems, there is a well-established method called intrinsic signal imaging (ISI). (Kalatsky and Stryker, 2003) ISI is a non-invasive brain imaging system that reveals a functional map of each mouse. ISI distinguishes V1 and up to 11 different higher visual areas (HVA) in the mouse visual cortex. (Garrett et al., 2014; Juavinett et al., 2017; Kalatsky and Stryker, 2003) With ISI, it is possible to accurately target visuo-cortical brain area of the mouse non-invasively before inserting an invasive electrical probe.

Together, the development of the Neuropixels probe, Kilosort2 and the ISI system offer unprecedented opportunity to accurately record thousands of neurons in multiple visual areas simultaneously. With this ability, I asked how different visual areas synchronize neural activity to process visual information. I chose to focus my analysis on neural oscillations, which have been implicated in synchronizing neural activity across multiple brain regions

Neural oscillations in the brain have been a subject of curiosity since they were first discovered from EEG data of human subjects, as alpha oscillation that appeared when subjects closed their eyes. (Berger, 1929; Buzsaki and Draguhn, 2004) Since then, neural oscillations have been found from various recording methods including single neuron recordings and extracellular field potentials, which are known to reflect synchronous neural population activity. (Buzsaki, 2004; Llinás, 1988) There is controversy over whether oscillations are simply a by-product of the brain's function or if the oscillation carry a

functional implication. (Buzsaki and Draguhn, 2004; Buzsaki and Wang, 2012; Fries, 2005) However, both perspectives accept the fact that there is periodic synchrony in neural activity.

In mouse visual areas, there is prominent gamma oscillation (narrowband gamma oscillation, NBG) found in the primary visual cortex, in the lateral geniculate nucleus (LGN) of the thalamus, and in the retinal ganglion cells. (Niell and Stryker, 2010; Saleem et al., 2017; Storchi et al., 2017) Work from our lab (Speed et al., 2019) has revealed that NBG in mouse primary visual cortex (V1) layer 4 contributes to the detection of a visual stimulus during a visual detection task. (Speed et al., 2019). Layer 4 in V1 is known to get direct visual input from LGN, which is the main source of retinal information to V1. Moreover, it is known that V1 inherits NBG from LGN (Saleem et al., 2017).

However, several questions remain unanswered about the functional role of NBG, including: 1) the existence of NBG in higher visual areas (HVA), 2) How coherent gamma oscillations are propagated in multiple visual areas, and 3) the role of NBG in mouse visual processing. Many of these questions can be answered with detailed neural data analysis of simultaneous recordings from multiple brain areas spanning across the thalamus, V1, and HVAs.

An open-source dataset – The Allen Visual Coding dataset – contains data from neural recordings of up to 6 simultaneous visual cortical areas revealed by intrinsic signal imaging (ISI) with Neuropixels probes, which are spike-sorted with Kilosort2, which I benchmark in the first half of this thesis. (Joshua H. Siegle, 2019) Hence, for the second half of this thesis, I study the above three unresolved questions about narrowband gamma

oscillation in visual areas by applying the validated methods to analyzing thousands of identified neurons (spikes) and population activity (local field potential, LFP) in visual areas.

CHAPTER 2. BACKGROUND AND METHODS

2.1 Background

2.1.1 Visual information propagation in mouse visual system.

Mouse visual information propagates from retina to lateral geniculate nucleus (LGN) of the thalamus, to primary visual cortex (V1). Then the information in V1 goes to higher visual areas (HVA). (Figure 1.)

2.1.2 Higher visual areas

Higher visual areas are the visuo-cortical areas that is not V1 and known to process visual information. These areas are suspected to perform higher-order processing of visual signals. (Glickfeld and Olsen, 2017) The use of intrinsic signal imaging enabled accurate targeting of distinct higher visual areas before measuring electrical activity. (Garrett et al., 2014; Glickfeld and Olsen, 2017; Juavinett et al., 2017) This allowed for many studies of anatomical and physiological structure of higher visual areas as well as functions. (Bienkowski et al., 2019; Glickfeld and Olsen, 2017; Harris et al., 2019; Murgas et al., 2020; Siegle et al., 2019; Vangeneugden et al., 2019).

Among various higher visual areas (Garrett et al., 2014), I focused analysis on these areas because there areas are the most clearly defined and Allen Visual coding dataset has extensive recording data (Garrett et al., 2014; Siegle et al., 2019) : LM (lateromedial area), RL (rostrolateral area), AL (anterolateral area), PM (posteromedial area) and AM (anteromedial area)

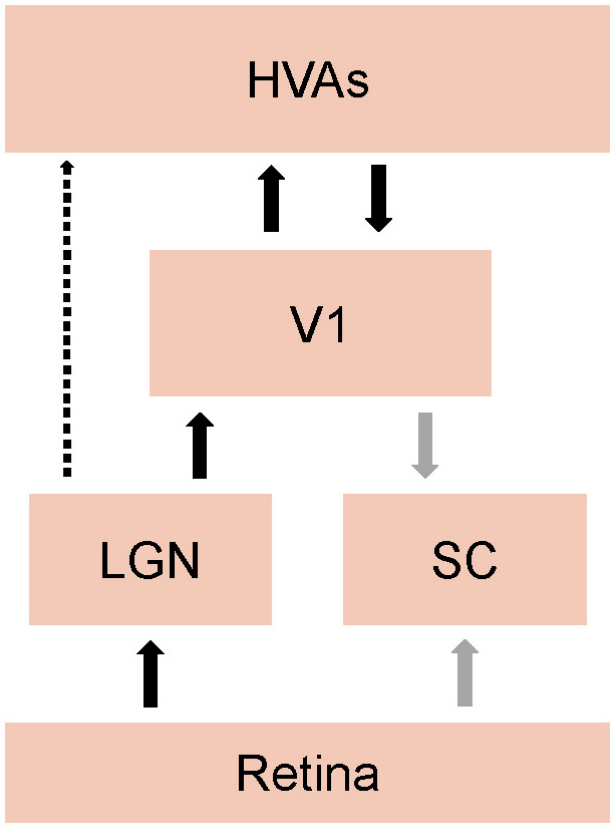

Figure 1. A schematic of visual information propagation of mouse adjusted from (Glickfeld and Olsen, 2017). Black lines are the information propagation that I consider in the thesis. Dotted line is non-conventional information propagation pathway.

2.1.3 Neuropixels 1.0 probe

Neuropixels 1.0 probe is multi-channel silicon probe that significantly increased the number of simultaneously recordable channel using CMOS (Complementary Metal Oxide Semiconductor) fabrication methods. (Jun et al. 16) Neuropixels 1.0 probe has 986 recording sites, and at most 384 channels could be used simultaneously. It spans at most 1cm in depth, which in the visual system, permits targeted recordings from cortex, hippocampus, and lateral geniculate nucleus simultaneously.

2.1.4 Action potential

An action potential is an electrical signal that is triggered by a neuron, that is known to be a fundamental unit of information. (Kandel et al., 2000) Action potential is also called a spike of a neuron. All action potentials result from a specific process: depolarization, hyperpolarization and repolarization of membrane potential which forms a specific waveform when measuring membrane potential across time.

2.1.4.1 Local Field Potential (LFP)

Local field potential is an extracellular field potential that is recorded inside the brain. (Buzsaki et al., 2012) LFP is calculated by lowpass filtering the raw extracellular recording to get low frequency fluctuation (typically < 200 Hz) caused by synchronized population activity of neurons. It is known that the driving force of the LFP is mainly due to synaptic currents between neurons. (Haider et al., 2016)

2.1.4.2 Spike-train

Neural spike-train is a vector of spike-times. It could be acquired with extracellular recordings followed by spike-sorting process as well as recording spikes with intracellular recordings. In neural analysis, usually spike-train is regarded as an activity of single/multi-neuronal activity and LFP is regarded as an activity of population of neurons.

2.1.5 Spike-sorting

Spike-sorting is a process that extracts neural spike-trains from the raw extracellular electrophysiological data. (Carlson and Carin, 2019) Due to its unsupervised nature, there are multiple algorithms, but no clear winner. It is known that the performance of different algorithms varies significantly with the types and conditions of the data. (Magland et al., 2020)

2.1.5.1 Calculation of Peri-stimulus time histogram (PSTH)

Peri-stimulus time histogram shows average neural response evoked by multiple repetitions of the same stimulus. It is computed by averaging neural activity of different trials such as LFP or spike-train on the stimulus onset. PSTH averages out single trial variability while maintaining the information regarding neuron's response to the stimulus.

2.1.6 Receptive field

The spatial receptive field of visual neurons corresponds to the region of space where visual stimuli elicit evoked action potentials. (Hubel and Wiesel, 1962)

2.2 Methods that were used throughout the paper

2.2.1 Kernel density estimation (KDE) on spike train

Spike-train is a sequence of binary events. Transforming spike-train to a spike-time histogram would convert to digital signal. For an accurate analysis of the signal, often converting to discrete time series is beneficial such as comparison with LFP, and when inferring baseline firing rate of a spike-train. Kernel density estimation is used to convert digital spike-time histogram to discrete time series. The output of KDE to a spike-train is regarded as a baseline firing rates of the spike-train.

2.2.2 Fourier analysis

Any real signal that has period P could be decomposed of weighted linear summation of sinusoids that have has period of P divided by positive integer. Fourier analysis is a way to represent signal by a linear summation of sinusoids. The process to find weights A_n of sinusoids of real signal s(x) is following (Oppenheim and Schafer, 1975):

$s(x) = \frac{A_o}{2} + \sum_{n=1}^{N} A_n \cos(\frac{2\pi nx}{P} - \theta_n)$ While $A_n = \sqrt{a_n + b_n}$ and

$a_n = \int_P s(x) \cos\left(2\pi x \frac{n}{P}\right) dx$, $b_n = \int_P s(x) \sin\left(2\pi x \frac{n}{P}\right) dx$

Fourier analysis is often used to approximate periodic signal. Especially the first harmonic is often used to find the neuron's responsive property to the periodic stimulus assuming cosine response function.

Fourier transform is one way of Fourier series decomposition that considers non-periodic signal as periodic signal with infinite period.

2.2.3 Fast Fourier transform (FFT)

Fast Fourier transform is an algorithm of performing discrete Fourier transform (DFT) or its inverse in computationally more efficient way. ($O(N^2) \rightarrow O(NlogN), where\ N = number\ of\ data\ points.$). (Oppenheim and Schafer, 1975) Fourier transform is a basis transformation from original domain to frequency domain. In other words, like Fourier series, it is a way to explain original signal with weighted linear summation of sinusoids while considering the period of the signal is infinite in Fourier transform.

2.2.4 Pearson correlation coefficient

Pearson correlation coefficient is a statistic that measures bivariate linear correlation between two variables. (Perkel et al., 1967) The value is between -1 and 1, that 1 indicates two variables are perfectly positively correlated and -1 indicates two variables are perfectly negatively correlated. The equation to compute Pearson correlation coefficient $\rho_{X,Y}$ is:

$$\rho_{X,Y} = \frac{cov\ (X,Y)}{\sigma_X \sigma_Y}$$

$$while\ cov()\ , and\ \sigma\ \ denotes\ covariance\ and\ standard\ deviation.$$

2.2.5 Cross-correlation

Cross-correlation is a measurement of correlation in the function of displacement of signal. In discrete signals, the equation of cross-correlation is:

$$xcorr(x, y) = \sum_{m=-\infty}^{\infty} x[n]y[m+n]$$

It is often used between two spike-time histograms to find the correlation with time lag between two spike-trains. Also, by appropriately normalizing two signals X and Y which makes mean to be 0 and standard deviation to be 1, it is possible to get Pearson correlation coefficient as a function of displacement.

2.2.6 Cell type identification with waveform width

The identification of neuron types was done by measuring the waveform width of the action potential. Here, the distance between the maximally depolarized peak and the maximally hyperpolarized trough is considered as waveform width. (Figure 2.) Then the distances are compared to the threshold (0.57ms). (Speed et al., 2020; Speed et al., 2019) If the distance is larger than the threshold, it is identified as putatively excitatory cell (regular spiking; RS), and if the distance is smaller, it is identified as a putatively inhibitory cell (fast spiking; FS). (Nowak et al., 2003; Speed et al., 2019; Speed et al., 2020)

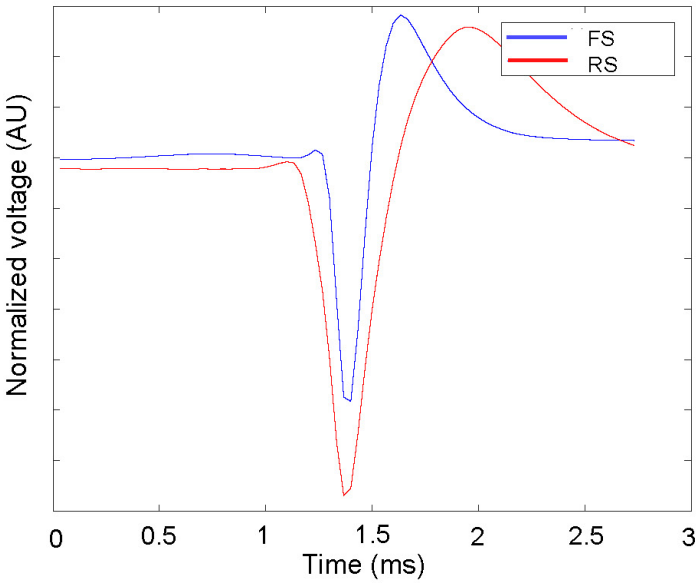

Figure 2. Average waveform of identified cell types spike-sorted with Kilosort2. Regular spiking cells (RS, putative excitatory neurons, N_{cell} = 121) have longer waveform than fast spiking cells (FS, putative inhibitory neurons, N_{cell} = 121). Cell types are identified with the waveform width, from trough to the peak of the waveform.

2.2.7 V1 layer4 identification with current source density (CSD)

The cerebral cortex is a laminar structure. (Buzsaki, 2004; Buzsaki et al., 2012) Each layer exhibits different anatomical and functional properties. Specifically, in primary visual cortex, layer 4 is known to receive visual input from thalamus.

In all types of neural activity, currents flow in and out of cells. (Mitzdorf, 1985). CSD applies second spatial derivative to the local field potential to get local current flow, and outputs areas the gets inward current flow (sink) and areas that gives outward currents (source). (Mitzdorf, 1985)

In the case of CSD on visual stimulus response, the earliest sink corresponds to the area that gets the earliest visual information. (Niell and Stryker, 2008; Speed et al., 2019) Since layer 4 is the area that gets visual input from thalamus, in CSD, the earliest sink channel corresponds to layer 4 of V1. (Figure 3.)

This method identifying layer 4 in V1 could not be generalized in HVAs because it is not known if HVA gets enough direct input from LGN, and also if the input layer is layer 4 or not. However, for consistency, for analysis that requires one LFP channel from HVA, I used earliest sink channel from HVA.

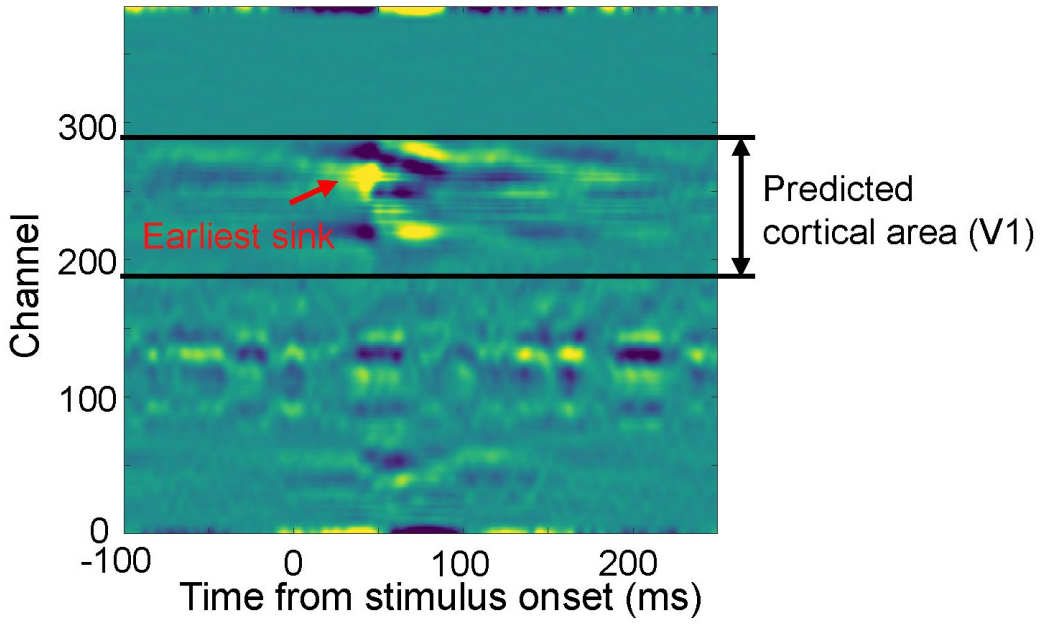

Figure 3. Example of stimulus triggered V1 current source density (CSD) using full field flash stimulus, from the Neuropixels probe. Cortex is top 1mm which corresponds to 100 channels of the Neuropixels probe. (Yellow: sink and black: source in the figure.)

CHAPTER 3. BENCHMARKING SPIKESORTING ALGORITHMS

3.1 Introduction

Spike-sorting is a process that extracts neural spike trains from the raw extracellular electrophysiological data. (Carlson and Carin, 2019) Action potential is considered as unit of information in the brain, thus the attempt to extract neural spikes from extracellular recording is essential in the field. (Carlson and Carin, 2019)

There are multiple spike-sorting algorithms in the field that use diverse methods. The problem with these algorithms is that they give significantly different result spike-trains from the same neural data. (Carlson and Carin, 2019) Moreover, there are spike-sorting algorithms that require manual manipulation after the automatic process which produces even more variant sets of result spike-trains from same neural data (Magland et al., 2020)

The quality of spike-sorting is difficult to quantify because collecting ground-truth data is difficult. There are two widely used methods on collecting ground-truth data: juxtacellular recordings which use simultaneous extracellular and intracellular recordings, and hybrid ground-truth that use only spikes that were previously spike-sorted. Each method has its own limitation, such as juxtacellular recordings being very difficult to perform, and nets one ground-truth neuron per experiment which limits the amount of data. The hybrid ground truth dataset is inherently limited by the performance of spike-sorting algorithm ability to generate a dataset.

This difficulty in having high quality ground-truth dataset caused the lack of amount of total available dataset. Hence, existing analyses focus on performance

considering general conditions such as types of probes, and cortical versus subcortical areas. (Buccino et al., 2019; Wouters et al., 2019) On the other hand, the performance of spike-sorting algorithm is highly variant in different conditions. For example, it is known that Kilosort2 has high performance at high channel count multi-electrode arrays data but poorly at tetrodes or lower channel electrodes data. (Magland et al., 2020).

Different brain regions have different types and density of neurons, firing rates and patterns. (Nowak et al., 2003) Hence, as different spike-sorting algorithms gives different results with types of electrodes, I hypothesized that the performance of the spike-sorting algorithms would vary with the specific brain region and behavioural states of the mouse (such as passively viewing stimulus or engaged to the task.). Specifically, I asked how different algorithms affects the scientific questions about single cell stimulus response statistics and the statistical detectability of short-latency pairwise neuronal interactions in mouse primary visual cortex with 32 channel multi-electrode probe.

3.1.1 Potential candidates: Kilosort2 and Klustakwik2

Klustakwik2 and Kilosort2 are spike-sorting algorithm developed in the same lab. (Pachitariu et al., 2016a; Rossant et al., 2016) Two algorithms use different methods of spike-sorting, hence they have distinct constraints and outcomes. The main difference of the known outcome of two algorithms is their ability to distinguish spikes that occur at the same time and same channel of the probe. (spatio-temporally overlapping spikes) Also, with high electrode count probes such as Neuropixels, Kilosort2 could perform spike sorting with acceptable computation time, while Klustakwik2 cannot handle the number of computations.

3.1.2 Haider lab extracellular electrophysiology dataset

Haider lab dataset is an invasive in-vivo neural recording dataset on mouse brain. It has times series of neural recording, timing information of stimulus presentation and mouse behavior such as lick timing and reward timing. Most of the dataset I use in this thesis is acquired with 32 channel single shank linear probe (Neuronexus A1x32) then spike-sorted with Klustakwik2 and Kilosort2. The dataset I used were ones that recorded primary visual cortex that spans all layers, which the mouse is has either passively shown a receptive field mapping stimulus or engaged to a behavioral task. (Speed et al., 2019; Speed et al., 2020; Williams et al., 2020)

3.1.2.1 Receptive field mapping using bar stimulus

Receptive field mapping is done with passive stimulus presentation of bar stimulus that is either vertical or horizontal bar to the contralateral hemifield. The bars are either white or black, 9° wide and spans -37.8° to 115.8° horizontallyin the visual space of the mouse. (Williams et al., 2020).

3.2 Methods

3.2.1 Overview

First, I spike-sorted the same recording with both Kilosort2 and Klustakwik2. The recordings were all done in head-fixed awake mice with Neuronexus probes targeted to V1. ($N_{recording}$ = 22, passive receptive field mapping stimulus presentation, $N_{recording}$ = 8, active behavioral task.) After spike-sorting, Haider lab members and I manually curated the spike-sorted results with Phy2. (Rossant et al., 2016) Only clusters with distinct

waveform shapes from other clusters in Phy2 output were considered as unique neurons. To identify putative same neuron among Kilosort2 and Klustakwik2, I considered neurons that had greater than 50% overlap of spike-times in the analysis. This criterion is less strict for a truly identical neurons, which I did to have statistical significance which requires large number of neurons. I compared single neuron receptive field statistics and detectability of pairwise interaction of putative same neurons between Kilosort2 and Klustatkwik2.

3.2.2 Single cell stimulus response statistics

Here, I compared stimulus response statistics of identified neurons. Receptive field is a fundamental property of neurons in V1 that require various types of analysis to fully understand. The properties that used on comparing are following: receptive field center/variance, response amplitude, response amplitude normalized by spontaneous firing rate and response duration. (Figure 4.)

3.2.2.1 Response amplitude

Response amplitude is a measurement of firing rate when the stimulus is present at the receptive field of the cell. I measured raw response amplitude and response amplitude normalized by spontaneous firing rate. (Figure 4. B)

3.2.2.2 Receptive field width

I fit Gaussian distribution on cell's response amplitude to stimuli presented at different positions in the visual field and took the standard deviation of the fit as a receptive field width. (Figure 4. B)

3.2.2.3 Receptive field center

I fit Gaussian distribution on cell's response amplitude to stimuli presented at different positions in the visual field and took the mean of the fit as a receptive field center. (Figure 4. B)

3.2.2.4 Response duration

Response duration is a duration of cell responding to the stimuli that is nearest to the receptive field center. Raw firing pattern was filtered with Gaussian kernel, and the duration was the period that the response was higher than half of the maximum firing rate of the response. (Figure 4. C)

3.2.2.5 Response latency

Response latency was measured by the filtered firing pattern first went above half maximum. (Figure 4. C)

3.2.2.6 Coefficient of variation (CV) of the inter-spike-interval (ISI) (Spikes in receptive field during the response)

Coefficient of variation (CV) of the inter-spike-interval (ISI) is defined as:

$$CV_{ISI} = \frac{std\ (ISI)}{mean(ISI)}$$

CV(ISI) is a metric to quantify spike regularity. In the stimulus driven model, spiking activity is more regular, so CV(ISI) is smaller. In the noise driven model, spiking activity is more irregular, so CV(ISI) is relatively larger. A different way of understanding is

CV(ISI) indicates how similar the spiking activity is to the Poisson process. If the spike generation process is a perfect Poisson process, CV(ISI) = 1, and if it's perfectly regular process, CV(ISI) = 0. (Qinglong Gu, 2020)

3.2.2.7 Fano factor of spikes in receptive field during the response

Fano factor is defined as:

$$Fano\ factor = \frac{var\ (spike\ count)}{mean(spike\ count)}$$

Fano factor is another metric to quantify spike regularity like CV(ISI). Unlike CV(ISI), Fano factor is using number of spikes in certain period, T. Spike generation process is often explained with the renewal process that accounts Poisson spike generation and get rid of spikes that disobey set refractory period. In the renewal process, if T goes infinity, the Fano factor and CV(ISI) becomes identical property that gives same output. (Destexhe et al., 2012)

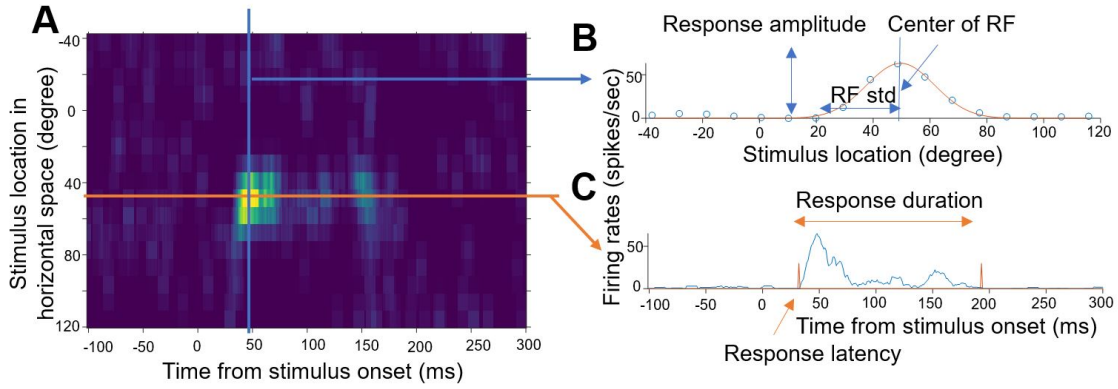

Figure 4. Summary of receptive field mapping properties.

A. Example color plot of an example single unit firing rate across different stimulus location and time. (yellow: high firing rate, black: low firing rate)

B. Response of the neuron in one specific time that has maximum response. Gaussian distribution was fitted to the data to get the response amplitude, center of receptive field and response standard deviation.

C. Response of the neuron to the stimulus location that maximally evoke response. Response latency denotes the time when the response first exceeds half of the maximum response amplitude. Response duration denotes the duration that exceeds half of the maximum response amplitude.

3.2.3 Statistical detectability in pairwise neuronal interaction

Here, I compared detectability in pairwise putative functional connectivity between cells measured with cross-correlation of two spike-trains. Specifically, I analyzed two types of interactions. First, I analyzed correlograms that had synchronized firing. In cross-correlogram these type of interaction shows peak at 0-time lag. I named this type of correlograms as time-synced functional connectivity. (TSFC) Second, I analyzed correlograms that showed synchronized firing with a constant time lag between them. In cross-correlogram these type of interaction shows narrow peak with short-latency. I named these correlograms time-lagged functional connectivity. (TLFC) For the analysis in this chapter, I focused more on time-lagged functional connectivity (TLFC) which could be subdivided to functional excitatory/inhibitory interaction. (Figure 6. A, B)

TLFC is identified by its shape and significance. The shape that I used to identify was narrow peak within short latency. Also, the correlogram was identified as putative functional connectivity if it crosses the significance threshold. The significance threshold was calculated using Poisson process. (Fujisawa et al., 2008; Senzai et al., 2019; Stark and Abeles, 2009)

3.2.3.1 Interpretation of pairwise neuronal connectivity

How to interpret TLFC anatomically has been debated for decades. Groups of people claims that TLFC it a monosynaptic connectivity (Fujisawa et al., 2008; Platkiewicz et al., 2019; Senzai et al., 2019; Stark and Abeles, 2009), and groups of people contradicts this by claiming that the correlation in firing pattern between neurons does not specify the

anatomical structure. (Cohen and Kohn, 2011; Das and Fiete, 2020; Kohn and Smith, 2005; Siegle et al., 2019)

In this thesis, my analysis was in support of the latter hypothesis, that time-lagged functional connectivity does not specify mono-synaptic connectivity. Anatomically, this functional connectivity could denote mono-synaptic connectivity but also a cascade of synaptic connectivity and delayed common input. I interpreted that the time delay between the activation of cells as a temporal correlation in activation pattern that contributes to the function of the neural circuit. Moreover, I distinguished excitatory and inhibitory interaction from the functional connectivity. Since the functional connectivity does not necessarily denote monosynaptic connectivity, I interpreted as in the local circuit, pre and post-activated neurons are positively (excitatory) and negatively (inhibitory) correlated in short time lag with narrow time window.

For the time-synced functional connectivity (TSFC), I interpreted as two neurons shares common input.

3.2.3.2 Reliable pairwise neuronal functional connectivity detection pipeline

These are the steps that I used to detect functional connectivity between pair of neurons:

a. Convert spike-train to spike-time histogram using 0.5ms bin.
b. Compute cross-correlation of spike-time histogram between neurons. (use -50ms to 50ms lag)
c. High-pass filter the correlogram with cutoff frequency of 70Hz to get rid of artefactual threshold crossing caused by lower frequency oscillations.

d. Convolve Gaussian filter with 4ms standard deviation on correlogram and set the output as a null hypothesis (If there is no correlation between neurons).

e. Use null hypothesis correlogram as mean of the Poisson process, compute 10^{-6} significance threshold.

f. If there is more than two consecutive points above the threshold only between 1.5ms to 4.5ms (including the border), it is identified as time-lagged functionally connected pair (TLFC). If two points above the threshold exists between 0-1.5ms (including the border), it is identified as time-synced functionally connected pair. (TSFC).

3.3 Results

3.3.1 Single cell statistics

3.3.1.1 Kilosort2 catches more spikes than Klustakwik2

The biggest difference between Kilosort2 and Klustakwik2 in single cell receptive field statistics is a receptive field response amplitude. Single neurons sorted with Kilosort2 had on average 1.5 times higher firing rates (in spikes/s), and 3 times higher when normalized to the spontaneous firing rate. (Figure 5. A, B)

With other metrics, receptive field center, width, response latency, response duration, Fano factor and coefficient of variation did not show significant difference between the results from Kilosort2 and Klustakwik2. (data not shown)

This suggests that Kilosort2 catches significantly more spikes than Klustakwik2, but not significantly biased in toward different functional properties of V1 neurons in passive bar receptive field mapping task.

I also analysed data of V1 when mice were engaged in a behavioural task. I found that this effect of Kilosort2 catching more spikes than Klustakwik2 was stronger when background firing rate was high. The effect was not significantly biased to behavioural task outcome (such as correct stimulus detection, failure in stimulus detection or false stimulus detection). (data not shown)

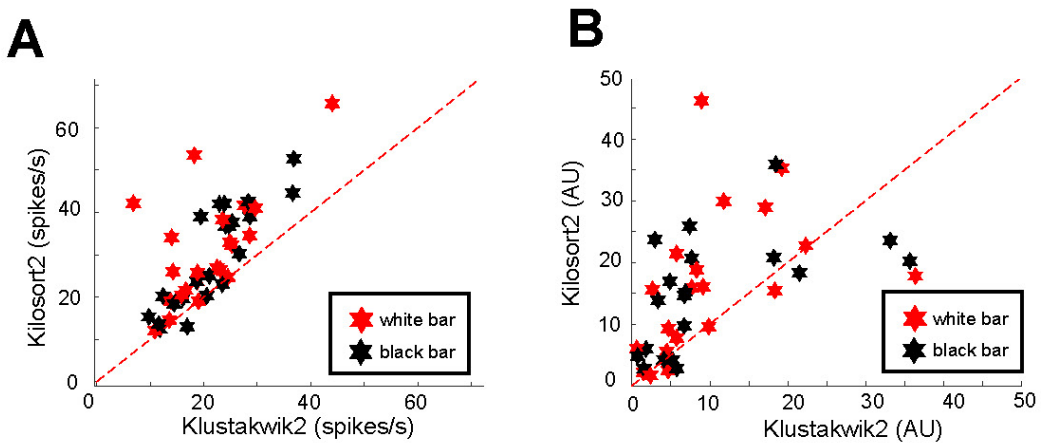

Figure 5. Kilosort2 catches more spikes than Klustakwik2. ($N_{recording}$ = 22)

A. Scatter plot of response amplitude to a visual stimulus inside the neuron's receptive field. (red: average response amplitude of single units from one session to white stimulus, black: same for black stimulus)

B. Same as A but response amplitude is normalized by spontaneous firing rate.

3.3.2 Pairwise cell statistics

3.3.2.1 Kilosort2 can detect more functional pairwise neuronal connectivity

Pairwise cell statistics were significantly different between the two algorithms. Kilosort2 had a 3 times higher probability of identifying time-lagged functional connectivity in both putative excitatory and inhibitory interactions. The main reason is that Kilosort2 has less false negatives because it can distinguish spatio-temporally overlapping spikes while Klustakwik2 cannot. Since detecting pairwise neuronal connectivity requires two spikes within 4ms or narrower window, ability to distinguish spatio-temporally overlapping spikes is essential.

Next, I quantified the limit of Klustakwik2's ability on detecting temporally overlapping spikes spatially. I quantified the number of artificial narrow trough around 0ms lag in the cross-correlogram that only occurred in Klustakwik2. I found the detection ability increases as spikes are spatially more separable with completely distinguishable temporally overlapping spikes when the source neurons were spatially separated by more than 160 microns (8 channels in Neuronexus A1x32 probe) (Figure 6. C)

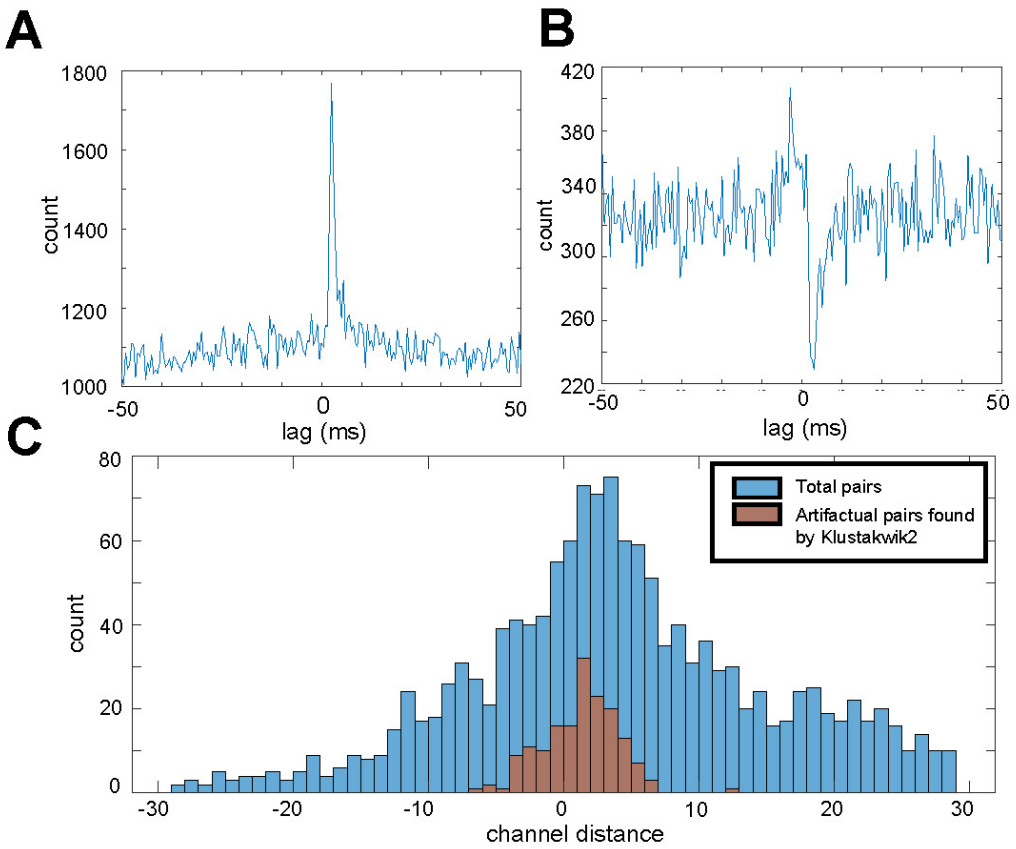

Figure 6. Kilosort2 is better at detecting time-lagged functional connectivity. ($N_{recording}$ = 22)

A. Example time-lagged functional connectivity here showing putative excitatory interaction revealed by cross-correlation of two neurons.

B. Example time-lagged functional connectivity here showing putative inhibitory interaction revealed by cross-correlation of two neurons.

C. (blue) Histogram of total pairs as a function of distance (estimated from the probe channel with largest action potential amplitude). (red) Histogram of pairs that had artifactual inhibitory TLFC that is spike-sorted with Klustakwik2. (The correlogram looks like in B but counts drops to 0 at 0ms due to inability of Klustakwik2 distinguishing spatio-temporally overlapping spikes as a function of distance.

3.3.3 Discussion

The existing surveys about the performance of spike-sorting algorithms considers types of probes and broad region of interest, such as if the area is cortical or subcortical. (Buccino et al., 2019; Magland et al., 2020) However, fewer studies have surveyed spike-sorting performance of different algorithms that could directly affect the conclusion of scientific question. (Laboy-Juárez et al., 2018) Hence, the goal of this project is to find out how would Kilosort2 and Klustakwik2 affect our lab's scientific question about neural information processing and visual stimulus response in visual cortex. Specifically, we started utilizing Neuropixels probe which Klustakwik2 cannot handle, and started changing the algorithm from Klustakwik2 to Kilosort2. Hence, I quantified the difference in spike-sorting output using Kilosort2 from Klustakwik2.

I found that Kilosort2 captures significantly mores spikes during stimulus presentation than Klustakwik2. This effect is stronger during high background firing. However, whether this result comes from Kilosort2 catching true spikes or false positive spikes is an open question. Also, I did not quantify how much is different during spontaneous, which I suggest to do in the future.

Spike-sorting is highly variant process which even with same recording, different algorithms find different putative neurons. (Magland et al., 2020) The ratio of putative same neurons over all identified neurons by either Kilosort2 or Klustakwik2 was less than 50%. Moreover, the criterion to identify putative same neuron was 50% overlap in spike-times, which is relatively mild for a truly identical neuron. I suggest how the result in this chapter changes with different criterion as a future verification step.

It is known that when mouse is engaged to active behavioural task, more neurons fire than when the mouse is passive. (Niell and Stryker, 2010) I found that also when mice are performing active task, Kilosort2 captures more spikes but I did not quantify how different it is. A valuable next step would be to quantify the spike-sorting performance during behavioural status such as task performance and arousal.

Another important finding is that Klustakwik2's ability in distinguishing temporally overlapping spikes within 8 channels ($160\mu m$) apart is highly unreliable; this limitation contributes to decreased detectability in pairwise functional connectivity. The effect is spatially biased, that could potentially contribute to the wrong conclusion to scientific questions. Hence, using Kilosort2 over Klustakwik2 is essential when interested in pairwise neuronal connectivity. (Kilosort2's ability in distinguishing spatio-temporally overlapping spikes is not perfect but the effect is much more spatially localized ($\leq 20\,\mu m$) and the temporally limited. ($\leq$ 1ms), which does not affect time-lagged functional connectivity. (TLFC))

Biases in spike-sorting could affect estimating neural population dynamics which is getting more popular with the ability of large-scale neuronal recording. (Vyas et al., 2020; Williamson et al., 2019) In estimating neural population dynamics, spike-sorting seems an essential pre-processing step because normally spike-train is an input to algorithms that estimates population dynamics. However, I predict the bias of spike-sorting algorithms such as Klustakwik2 in detecting synchronized firings from multiple neurons could also give rise to artefactual result in precise population dynamics. To cope with this problem, (Trautmann et al., 2019) proposed a temporary solution of using threshold crossing of extracellular recording from each electrode to infer neuronal population

dynamics. They found that using simple threshold crossing can estimate as accurate neural population dynamics result as using spike-trains from spike-sorting algorithm. However, great majority of scientific questions about neural population dynamics also requires information about the units that consists the dynamics which limits the finding of (Trautmann et al., 2019). Hence, a valuable next step would be to validate and quantify how spike-sorting algorithms affect to estimating neural population dynamics

Even though this study gave only limited results, I carefully conclude that the transition in the lab from Klustakwik2 to Kilosort2 is beneficial. I suggest three reasons: Kilosort2 has less false-negative especially during high background firing rates that would happen during active behavioural task, has ability to capture more abundant and accurate pairwise connectivity and has ability deal with larger channel count probes.

CHAPTER 4. REVEALING HIGHER VISUAL AREAS ACROSS CORTEX

4.1 Introduction

Intrinsic signal imaging (ISI) is a non-invasive brain functional imaging method that uses visible light to get functional map of the brain. It finds active brain areas by leveraging the fact that the brain surface reflectance of light changes with the oxygen level of blood. To find a functional map, standard input-output approach applies. Stimulus in various visual fields were shown, while simultaneously measuring reflectance of the light from the cortical surface. (Kalatsky and Stryker, 2003)

ISI is widely used in mouse experiments because mice have a thin skull that the visible light could penetrate into. For electrophysiology, a highly invasive and spatially localized neural recording method targeting the area of interest reliably before inserting probe is crucial. ISI is a non-invasive method that identifies the area of interest, by providing precise functional map of each individual mouse.

Development of ISI system requires system to acquire the signal, and post-process the acquired signal to compute functional maps. My project focused on post-processing the acquired signal to compute functional maps. It includes:

1. Compute retinotopic map from the acquired video and visual stimuli using Fourier analysis.
2. Calculate visual field sign map to separate distinct visuo-cortical areas.
3. Align of retinotopic map to vasculature of the mouse.

The result was then verified with previously reported ISI results from various literature. (Garrett et al., 2014; Juavinett et al., 2017; Kalatsky and Stryker, 2003)

4.1.1 Blood-oxygen-level-dependent imaging

High firing neuron requires high energy. To supply energy, blood needs to be concentrated near the neurons, and supply oxygen that results in the transformation of oxy- haemoglobin to deoxy-haemoglobin. Blood-oxygen-level-dependent (BOLD) imaging detects changes in blood oxygen level.

ISI that I used here detects deoxy-haemoglobin concentration change with red light (wavelength = 610nm) because in that wavelength deoxy-haemoglobin has much higher absorbance. For a reference map I used green light (wavelength = 525nm that has identical absorbance to both oxy and deoxy-haemoglobin), that reveals vasculature. (Sheth et al., 2012).

4.1.2 Retinotopic map

If the adjacent points in the visual field are represented by neurons in adjacent areas, the area is retinotopically organized. (Kandel et al., 2000) Visual cortex is retinotopically organized and the map that shows the receptive field of neurons is called a retinotopic map. (Figure 8. A, B)

4.1.3 Visual field sign map

It is known that visual cortex is retinotopically organized. Among different visuo-cortical areas, some visuo-cortical areas preserve original visual field, and the others have

mirror image of the visual field in its retinotopy. This means different visuo-cortical areas have different visual field signs. (Figure 8.C, D) (Garrett et al., 2014; Zhuang et al., 2017) For example, primary visual cortex preserves original image of visual field in the retinotopic map, while RL has mirror image. Hence, with this knowledge that different visuo-cortical areas have different visual field sign, it is possible to localize specific visuo-cortical area with visual field sign map.

4.1.4 Alignment of functional map on top of vasculature image

After acquiring retinotopic map, it is necessary to align the computed map on a visible indicator for actual experimental use of the acquired map. The most straight forward indicator for an experimenter is a vasculature on the skull which does not change day to day. Hence, I aligned functional maps on the vasculature image.

Specifically, alignment of the acquired functional map on top of vasculature image is used in four cases. First, it indicates where acquired retinotopy locates in the mouse visual cortex to the experimenter before inserting probe. Second, precise alignment is necessary for acquiring visual field sign map with both horizontal and vertical retinotopic maps. Third, alignment is crucial in merging multiple experiments that are recorded in either different recordings or different days to get improved quality retinotopic map. Fourth, the identified locations of functional map were subsequently directly compared with electrical activity of the LFP recorded from populations of neurons. This is an analysis to confirm if the hemodynamic response from ISI highly correlates with electrical signal recorded from neurons.

4.2 Methods

4.2.1 Retinotopic mapping

The main obstacle of using blood-oxygen-level-dependent (BOLD) signal to get the functional map of the brain is hemodynamic delay. Unlike the electrical signals that directly reflects the activity of neuron, blood oxygen level responds with variable delay of several seconds after neuron's activity. Not only that the delay is several seconds, the variability makes difficult to interpret the signal. Hence, traditional approach using episodic stimuli and time-series analysis to find region that responds to stimuli is inherently limited by the variable delay.

Interestingly, bi-directional periodic horizontal and vertical bar stimulus with Fourier analysis suggested in (Kalatsky and Stryker, 2003) is known to be relatively robust to the variable haemodynamic delay which we adopted to use. (Schematic of general experiment is in Figure 7.) This method has two assumptions. First, within each area (pixel in the map) and each recording, the delay is constant. Second, neuronal population activity of the region of interest does not have directional bias, so the forward and backward run of the stimulus presentation is symmetric. (Kalatsky and Stryker, 2003)

Periodic stimulus could denoise activity outside of the period of the visual stimulation. We used the period of the stimuli, 18 second, that is outside of other inherent periodic oscillations of blood flow activity such as heart beat, (2-5Hz), respiration rate (0.3 – 1 Hz) and vasomotor signal (0.05-0.1Hz). Furthermore, bi-directional stimulation is able to cancel out hemodynamic delay through its symmetry.

The detailed processing steps to achieve retinotopic map is following. The acquired video is in the dimension of (x pixels, y pixels, time). First, the image subtracts the mean 2D image to get rid of DC components. Then, first harmonic response to visual stimuli of each pixel is calculated to get the phase of the first harmonic. In other words, Fourier transform was performed and the value that has frequency of stimulus is used for analysis. The phase of the first harmonic is regarded as each pixel's receptive field added with hemodynamic delay. (For the forward stimuli, $\theta_{forward} = \theta_{recpet} + \varphi_{delay}$)

In order to get rid of the hemodynamic delay, we used symmetric backward presented stimuli as well. Same processing step was performed to each pixel. The result phase of the first harmonic is the inverse of each pixel's receptive field plus hemodynamic delay. ($\theta_{backward} = 2\pi - \theta_{recpet} + \varphi_{delay}$)

Finally, subtracting backward run phase from forward run phase and divide by 2 gives the receptive field of each pixel. ($\theta_{foreward} - \theta_{backward} = 2\pi + 2\,\theta_{recpet}$, which is equal to $2\,\theta_{recpet}$ by periodicity. Then dividing by 2 gives θ_{recpet}.) In conclusion the receptive field property was calculated by $\theta_{recept} = \frac{\theta_{forward} - \theta_{backward}}{2}$. (Kalatsky and Stryker, 2003)

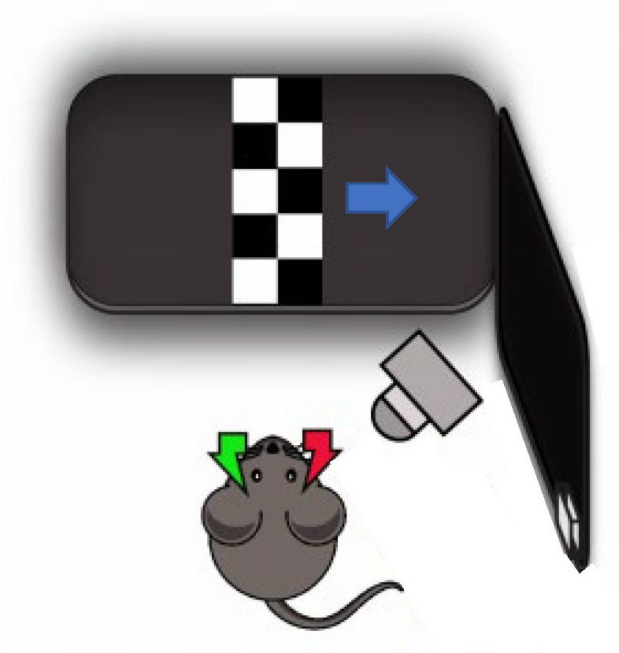

Figure 7. Experimental set up of intrinsic signal imaging system. (Figure adjusted from unpublished work from the lab)

Mouse is anesthetized and head fixed. For functional mapping, only red light is present and the camera is taking a video of the skull with sampling rate of 10Hz. (Green light is used to visualize the vasculature) A moving checkerboard bar stimuli is presented to the mouse with the period of 18s. (Forward run direction denoted as an arrow). At the same time, a photodiode is measuring each event times such as start of the recording, start of the stimuli and the end.

4.2.2 Visual field sign map

The acquired retinotopic maps of vertical and horizontal visual field are used to get visual field sign (VFS) map. VFS map has VFS at each pixel that is acquired by computing the difference between spatial gradient direction of vertical and horizontal retinotopic maps. The equation to get visual field sign S is following:

$$S = \sin(\angle \nabla V - \angle \nabla H)$$

$\angle \nabla V \ and \ \angle \nabla H$ are the gradient direction of vertical and horizontal retinotopic map. (Garrett et al., 2014) (Detailed methods and explanation are in Garrett et al. 2014)

4.2.3 Alignment of functional map on top of vasculature image

There are two types of alignment. The first type of alignment is to place functional map on right anatomical location. Second type is to align the two vasculature images from different recordings to merge retinotopic maps to improve the quality of map. For the both of the alignment types, I made three assumptions:

1. The distance between the camera and the cranial window is consistent across experiment. i.e. the size of the map does not change across the experiment.
2. ISI camera does not rotate in any experimental situation.
3. Within one recording session, ISI camera does not move its position and angle.

Alignment was performed in three steps. First, I get rid of unnecessary rows and columns that are outside of the cranial window. (Figure 9.A) Second, each of two images subtracted mean of each image than divided by the standard deviation image. Third, I crop both images to match the size of images by selecting rows and columns that minimizes the Euclidean distance of two images.

4.3 Results

4.3.1 Retinotopic map and visual field sign map

With the sufficient repetition of periodic stimulus, I was able to get vertical and horizontal retinotopic map and VFS map. (Figure 8. A, B, C) The retinotopic maps had clear continuous retinotopy spans monocular and binocular visual field that were shown. Also, the gradient of the retinotopy is perpendicular in horizontal and vertical receptive field that is consistent with the literature.

Then, the calculated VFS maps were compared with the literatures. (example VFS map in Figure 8. D) (Garrett et al., 2014; Juavinett et al., 2017; Zhuang et al., 2017) General structure of the acquired VFS map is consistent with VFS map in Zhuang et al. 2017. Compare to the VFS map in Zhuang et al .2017, the location of V1, LM, RL and PM is very clearly shown in our result, the location of AL and AM are less clear but still inferable.

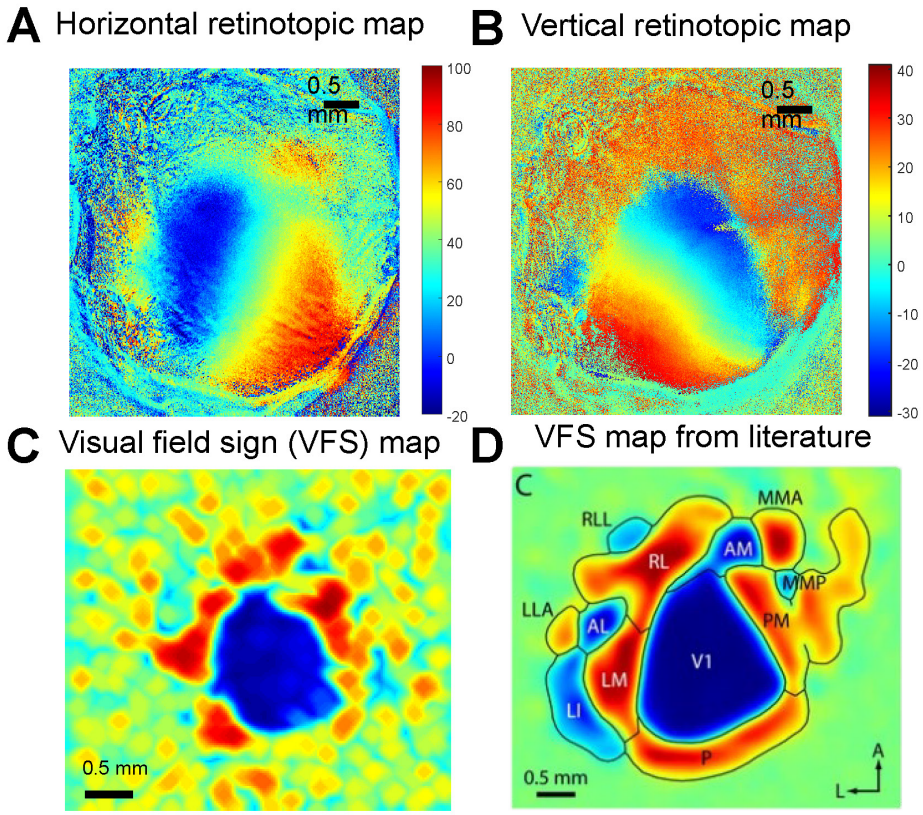

Figure 8. An example of acquired functional maps from ISI.

A. Retinotopic map of the horizontal visual field of the mouse. The color axis denotes the angle in the horizontal visual field.

B. Retinotopic map of the vertical visual field of the mouse. The color axis denotes the angle in the vertical visual field.

C. Example visual field sign map that was calculated with A and B.

D. Example visual field sign map from Zhuang et al. 2017.

4.3.2 Alignment is accurate.

The alignment error is less than 30 μm within same day experiment and 75 μm within different day experiment. (Figure 9. $N_{mouse} = 1, N_{recording} = 3$) However, an angular noise potentially from rotational movement of the camera was found, contrary to assumptions made. (Figure 9. B, C.)

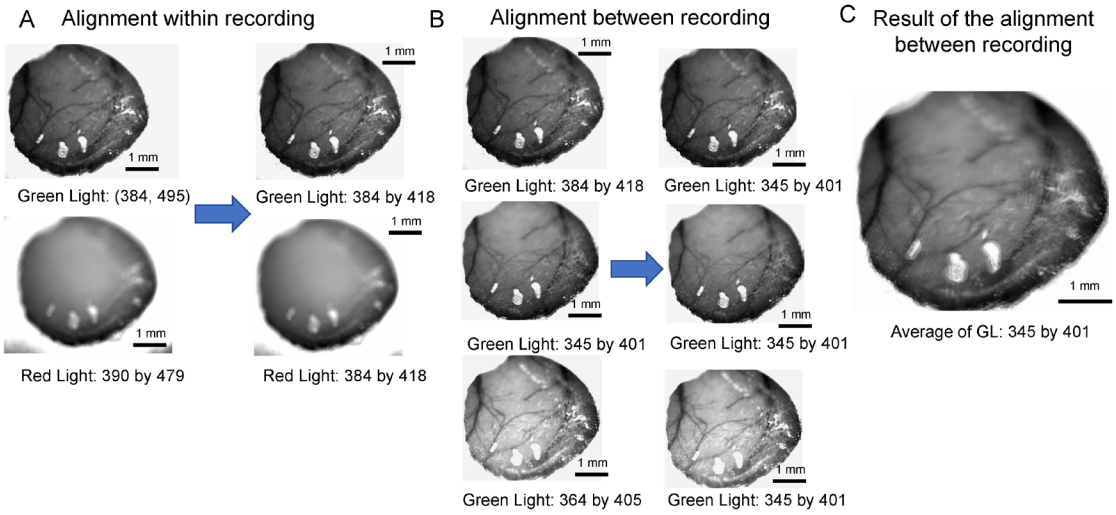

Figure 9. Alignment of functional maps and merging different recordings.

A. Matching the size (Alignment) between the vasculature frame (Green light, top) and the first frame of the functional map (Red light, bottom) in the same session. Numbers below the figures denote size of frames in pixel. Maximum aligning error is less than 2 pixels (30μm).

B. Matching the size between different vasculature frames that were recorded in different days. Maximum error is less than 5 pixels (75μm).

C. The average of three different vasculature frames on the right side of B. There is a blurry effect because of the angular noise.

4.4 Discussion

Advances in behavioural and systems neuroscience have resulted in a surge of experiments where training mouse to a behavioural task for weeks and simultaneous recording is becoming more common. The failure in targeting the desired brain area accurately is costly in mice that have significant experimenter investment in behavioural task training. ISI provides functional map of individual mice to the experimenters. Hence, the development of generating retinotopic map and VFS made possible for experimenters to know the area of interest before inserting probes, minimizing costly experimental errors in targeting recording sites.

The acquired retinotopic map and visual field sign map were consistent with the maps from previous literature. The automatic alignment algorithm of the functional map to the vasculature was accurate that usually had only few tens of micron error. Also, comparison with LFP recording reassured that the retinotopic map from hemodynamic response reflected neural receptive fields.

Retinotopic maps that I calculated needed more repetitions for good quality result compared to ones in the literature. I hypothesized two reasons. First, the post-processing pipeline is non-optimal. I found small error in sampling frequency from what we used in doing Fourier transform. I interpolated the frequency domain signal to get exact frequency which did not change the result. Also, I found acquiring video is not perfectly uniformly sampled while post-processing assumes uniform sampling. Hence, I got the time points each sample was acquired, and tried non-uniformly sampled FFT, but the change was trivial.

Second, the result from literature is with mice with skull removed while our result is with skull intact. Skull reflects significant amounts of signal, which attenuates SNR, which could require more repetition to get same quality when skull is removed. However, we did not record mice without skull to verify this hypothesis. I suggest it for a valuable future work verification step.

There is inherent limitation of ISI. ISI is stimulus dependent process, so with visual stimulus, it is only possible to reveal functional map of visual cortex. The field is moving to multi-modal area recording, ISI couldn't be used in areas out of visual cortex without changing the stimulus modality (e.g. auditory or somatosensory).

The lab is continuing this line of research by quantifying the variability of the ISI system in different visuo-cortical areas. This research aims to quantify how variable ISI is, how noisy and how repeatable the result is. Finding how to reduce the noise level would be a good next step.

In the future, since computational ability is not a bottleneck anymore, it would be beneficial to use more than the first Fourier harmonics. With the current approach that uses only the first Fourier harmonic is assuming that the stimulus tuning to bar stimulus is cosine. Physiologically it is true for V1 but it is not for areas other than V1. Hence, with current approach it is not guaranteed the phase found from ISI would actually denote the receptive field of the area. Hence, implementation of phase detection with all possible Fourier harmonics would be required for accurate analysis, and it would not only improve the quality of ISI drastically but also reduce number of repetitions needed and show distinct visual tuning of different visuo-cortical areas.

CHAPTER 5. NARROWBAND GAMMA OSCILLATION ACROSS MOUSE BRAIN

5.1 Introduction

5.1.1 Allen institute visual coding dataset

Allen Institute visual coding dataset is a systemic survey of spiking activity in the mouse visual system including cortex, thalamus and hippocampus. (Siegle et al., 2019) It acquires spiking data from awake mouse with up to 6 simultaneous Neuropixels recording. Each probe target V1, LM, RL, AL, PM and AM respectively, and these probes go deeper than cortical areas to subcortical areas, with a subset of them successfully recording activity in LGN and LP (lateral posterior; higher-order visual thalamus) in thalamus and hippocampal areas. For my analysis, I analyzed spiking activity in all 6 visuo-cortical areas and LGN in thalamus. (Figure 10. B. Figure 2 from (Siegle et al., 2019))

While recording, mice are exposed to various set of visual stimuli. (Detailed explanation in white paper. (Siegle et al., 2019)) For my analysis, I focused analysis on 100% positive/negative contrast full field flash, and drifting Gabor grating stimulus with different drifting direction.

In Allen Institute visual coding dataset, each mouse has been recorded only once to localize the inserted probe accurately. (Siegle et al., 2019)

5.1.1.1 Full field flash

Each recording contains 75 presentations of both positive/negative full field flash, for 250ms. The Inter-stimulus interval is 1750ms. During inter-stimulus interval, grey screen was presented.

5.1.1.2 Drifting grating

In each recording, there is more than 600 presentations of drifting grating. This includes full contrast and 0 contrast (blank) drifting grating stimulus. The duration of the stimulus is 200m0s and inter-stimulus interval is 1000ms.

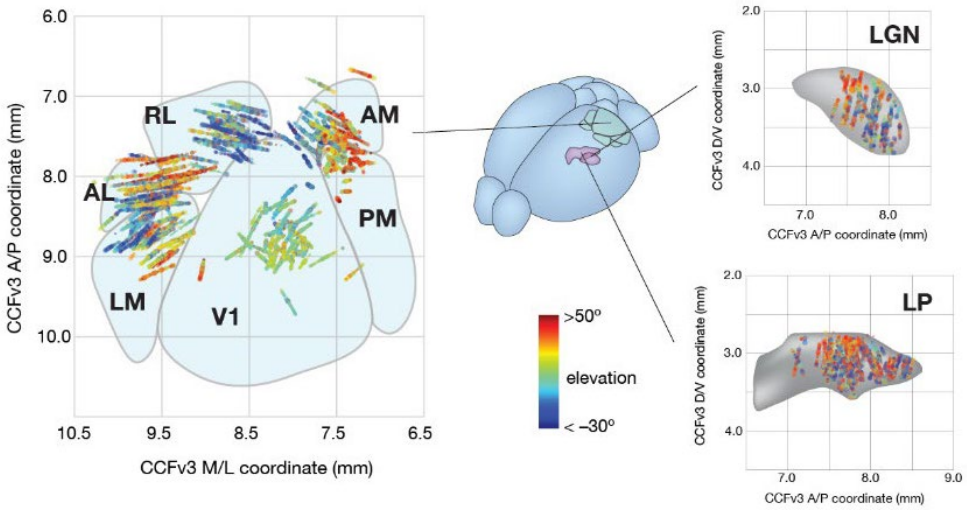

Figure 10. Allen Institute Visual coding dataset summary figure from Figure 2 in (Siegle et al., 2019). Up to six Neuropixels probes targeted six visuo-cortical areas respectively. Dots represent location of neurons aligned with Allen common coordinate framework. Different color denotes receptive field of the neuron. Subset of neurons penetrated cortex and reached to LGN and LP (lateral posterior) in the thalamus.

5.1.2 Narrowband Gamma Oscillation

Narrowband Gamma oscillation (NBG) is as a periodic fluctuation of brain activity between 50-70 Hz specific to mouse visual area. NBG is first studied by (Niell and Stryker, 2010). They recorded V1 LFP and found NBG is prominent in V1 and promoted by locomotion and suppressed by visual contrast. (Niell and Stryker, 2010)

The study was followed by (Saleem et al., 2017). Researchers recorded V1 and LGN, and found NBG power is enhanced with increasing luminance and arousal and suppressed by visual contrast. (Saleem et al., 2017) Also, NBG could be detected in the spiking activity of LGN as well. Auto-correlogram and cross-correlogram of spike-sorted clusters exhibits NBG. (Saleem et al., 2017) In single cells in LGN, NBG is coherent and it is thought that this coherence enhances visual signaling. (Saleem et al., 2017; Storchi et al., 2017)

NBG is inherited from retina (Storchi et al., 2017) and propagates to LGN to V1 through excitatory neurons, in feedforward pathway. (Saleem et al., 2017) Especially, NBG in V1 disappears when LGN is inactivated, (Saleem et al., 2017) and NBG in retina disappear when intrinsically photosensitive retinal ganglion cells (ipRGC) are inactivated. (Storchi et al., 2017)

NBG has been rarely studied in terms of mouse behavior. A study from our lab (Speed et al. 19) found that in visual detection task, trials of correct stimulus detection had higher pre-stimulus NBG power in V1 layer 4 than trials of incorrect detection. This finding suggests the possibility that NBG promotes detection of visual stimulus.

5.1.3 Broadband Gamma Oscillation

Broadband Gamma oscillation (BBG) is a periodic fluctuation of brain activity typically between 30-90Hz that exists in mammalian cortex. (Buzsaki and Wang, 2012; Fries, 2009, 2015) BBG in cortex is thought to have distinct mechanisms. For example, BBG benefits sensory processing through precise synchronized activity of inhibitory neurons. (Fries, 2009; Saleem et al., 2017; Siegle et al., 2014; Tiesinga and Sejnowski, 2009) BBG gives periodic "windows of opportunities" to pyramidal neurons that relay stimulus information by periodically giving lowest inhibition from synchronized inhibitory neuron activity. (Siegle et al., 2014) In the mouse visual cortex, BBG is modulated with stimulus formation especially is enhanced with visual contrast. (Saleem et al., 2017).

In this thesis, my main focus is NBG. Hence, I used BBG as a control for investigating NBG. I restricted the frequency of BBG to non-overlapping with NBG. (30-50Hz)

5.1.4 Intrinsically photosensitive retinal ganglion cells (ipRGC)

It is thought that NBG in the brain originates from retina. (Koepsell et al., 2009; Saleem et al., 2017; Storchi et al., 2017) Within retina, intrinsically photosensitive retinal ganglion cells (ipRGC) are known to modulate NBG in the visual system. (Storchi et al., 2017) by increasing firing rates with luminance. (Do, 2019)

ipRGC has photosensitive protein, melanopsin which makes ipRGC photosensitive without receiving input from rods and cones like other retinal ganglion cells . (Huberman and Niell, 2011).

Multiple functions of ipRGCs to visual and non-visual functions have been suggested. That includes regulating circadian rhythm, pupillary light reflex. (Do, 2019)

5.1.5 Questions and hypothesis of NBG

I am trying to answer three large questions about NBG in this thesis. First, would visual areas other than LGN and V1 exhibit NBG? This question is highly relevant in hypothesizing the role of NBG in sensory processing. If NBG is only in an early visual stage, it would have simpler role, while if it is also in HVA, it would be more likely to perform more complex role in visual processing. To answer this question, I analyzed electrical activity of LGN, V1, and the higher visual areas RL, LM, AL, AM and PM during spontaneous activity and stimulus presentation.

The next question is how NBG is propagated in multiple visual areas. With initial analysis, I found that NBG is present in HVAs. With correlation analysis, I found in some recordings, correlation between LGN and HVA was higher than correlation between LGN and V1. This contradicts with the known visual pathway that visual information propagates from LGN to V1 to HVA. Hence, I was curious about what route NBG in HVA is propagated from LGN.

The last question is what would be the role of NBG. The results of previous literatures have suggested three hypotheses on the role of NBG. First, (Saleem et al., 2017) suggested NBG as an idling rhythm. Since NBG is active during spontaneous and suppressed to visual contrast, they suggested NBG is in visual system to represent idle status. Second, the other hypothesis they suggested is NBG as a channel for thalamo-cortical, and cortico-cortical communication, that is consistent with the hypothesis

suggested as the role of neural oscillations. (Fries, 2015) Third, (Storchi et al., 2017) suggested the coherence of NBG within cells promotes visual signaling of luminance information. Also, (Speed et al., 2019) did not explicitly mention a novel hypothesis, but suggested NBG during the pre-stimulus period could improve the mouse's ability to detect visual stimuli.

From hypothesis suggested from previous literatures and result of my own analysis I hypothesized two potential roles of NBG. First, I hypothesize NBG synchronizes excitability of retinal-thalamo-cortical pathway and provides "window of opportunity" for sensory information to be propagated. (Fries, 2015; Saleem et al., 2017)

Second, I hypothesize NBG encodes luminance information in the early visual system in a computationally convenient and efficient way. (Storchi et al., 2017).

5.1.6 Methods

5.1.6.1 Cycle histogram

Cycle histograms reveal the level of coherence of the selected frequency band of the LFP and the timing of spikes. This method aligns spike to each cycle of bandpass filtered LFP. The detailed steps for calculating cycle histograms is the following:

1. First, I bandpass filtered the LFP and found the location of peaks (local maxima) of the filtered LFP.
2. Then, I defined a period of the oscillation as peak to peak.

3. Lastly, I aligned the spikes to the phase of period of the oscillation and acquired histogram of phase location of the spikes. (Example cycle histogram in Figure 15. A)

5.1.6.2 Spike triggered local field potential

As PSTH is a triggered average on stimulus onset, spike triggered LFP is a spike triggered average LFP.

5.1.6.3 Short time Fourier transform

Short-time Fourier transform (STFT) is a widely used method to reveal how spectral components of signal evolves in time. STFT consists two parts, windowing and Fourier transform. Windowing is a way to segment time-domain signal. A convenient way is to use a rectangular window, that it just split time-domain signal into multiple segments. A better way of windowing is to use windows that account for edge effects such as Hamming or Kaiser window. Then each segment is Fourier transformed. Usually STFT is plotted with time-frequency spectrogram.

5.1.6.4 Hilbert transform

Hilbert transform is a method that recovers imaginary part of the hypothetical complex signal. It is often used to identify instantaneous amplitude of the oscillation and instantaneous phase of the narrowband oscillation.

5.1.6.5 Identification of cells exhibit narrowband gamma in visual areas

I identified cells that exhibit NBG in their spike-trains and identified these as NBG cells. I analyzed auto-correlograms and cross-correlograms between every cell in one recording. If any of correlogram has prominent 50-70Hz power in the spectral domain, I identify these as pairwise NBG pair.

Since spectral power of spike-train does not follow usual 1/f relationship in LFP (Saleem et al., 2017), residual NBG power is defined heuristically. The NBG power should fulfill two conditions:

1. NBG power should be higher than the z value of power between 30 to 150Hz.
2. NBG magnitude should be higher than maximum magnitude within 150 to 1000Hz

From putative NBG pairs, I identified both cells from the correlogram that shows prominent NBG power as NBG cells. (Figure 11. example correlograms of NBG cells and one example cell, and correlograms of non-NBG cells and one example cell.)

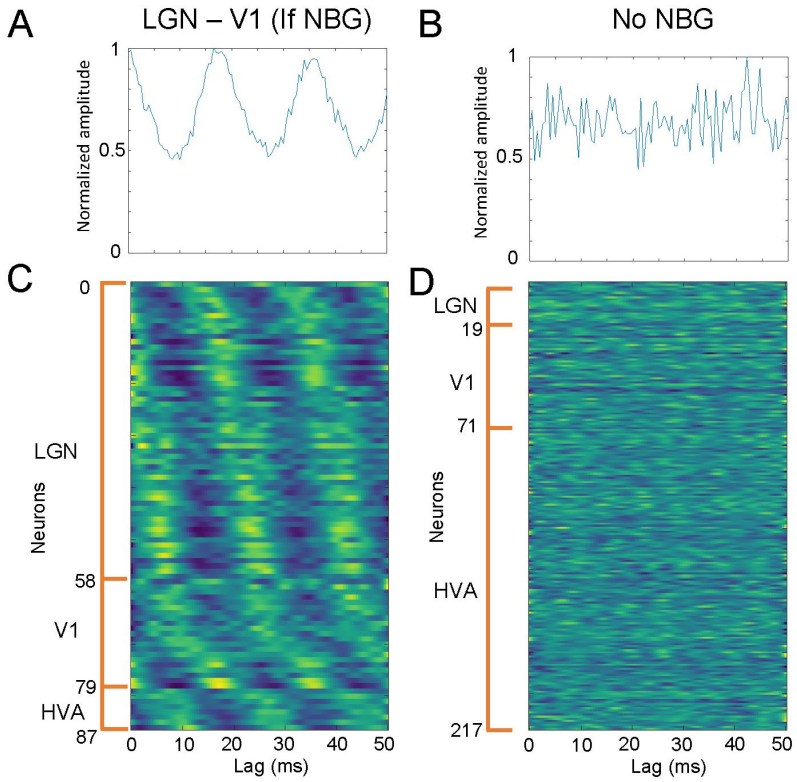

Figure 11. Identification of "narrowband gamma" cells across thalamo-cortical visual areas using pairs in one example recording. (N_{cell} = 304)

A. Example cross-correlogram between cells during spontaneous activity that shows narrowband gamma oscillation. If the auto/cross-correlogram exhibits NBG, I classified both of the cells as "narrowband gamma" cells.

B. Example cross-correlogram between example "narrowband gamma" cell and non-"narrowband gamma" cell during spontaneous activity.

C. Cross-correlogram of one example "narrowband gamma" cells and all other "narrowband gamma" cells recorded in LGN (N_{cell} = 58), V1 (N_{cell}= 21) and HVA (N_{cell}= 8) in one example recording.

D. Example cross-correlogram between example "narrowband gamma" cell (same cell from C) and all of non-"narrowband gamma" cell in the example recording.

5.2 Is narrowband gamma oscillation present in higher visual areas?

5.2.1 Methods

5.2.1.1 Current source density to identify earliest response layer of higher visual area.

For the analysis to find if HVA population activity exhibits NBG, I focused on the layer that exhibits earliest stimulus response. This comes from the assumption that if HVA exhibits NBG, this comes from feedforward pathway from V1 or the thalamus. Unlike the earliest sink layer of V1 that is assumed to be layer 4, which layer in HVA exhibits first visual response is unknown. I used current source density analysis of stimulus trigger averaged LFP of the probes that goes to HVA to find the earliest sink layer of the area that exhibits the earliest stimulus response. The example CSDs of different visuo-cortical areas are in Figure 12.

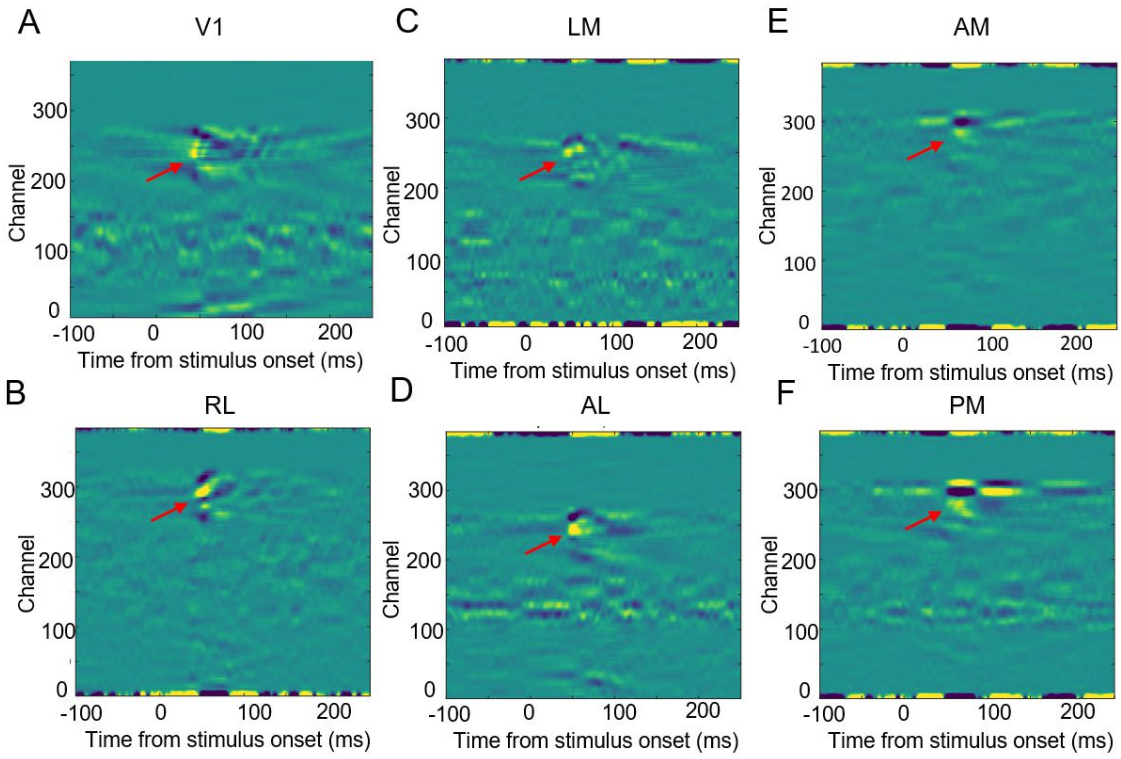

Figure 12. Finding the earliest stimulus response channel of the visuo-cortical area through current source density. (Each example with one recording)

CSD was computed with full field flash stimulus on probes in different visuo-cortical areas. Red arrow denotes the earliest sink channel of the CSD which corresponds to earliest stimulus response channel. (Yellow: sink and black: source)

A. **CSD of a probe in V1. (Earliest sink channel = 240, latency = 38.4ms)**

B. **CSD of a probe in RL. (Earliest sink channel = 291, latency = 42.4ms)**

C. **CSD of a probe in LM. (Earliest sink channel = 252, latency = 42.4ms)**

D. **CSD of a probe in AL. (Earliest sink channel = 241, latency = 44.8ms)**

E. **CSD of a probe in AM. (Earliest sink channel = 284, latency = 56.8ms)**

F. **CSD of a probe in PM. (Earliest sink channel = 280, latency = 50.4ms)**

5.2.2 Results

5.2.2.1 NBG exists across all higher visual areas

5.2.2.1.1 NBG exist in pairwise neuronal functional connectivity

Understanding how NBG is represented within single cells spikes is important. Since spike is a binary event, raw single unit spike-train has negligible NBG signal. Hence, I used cross-correlation and auto-correlation to reveal NBG in spikes. If there is shared NBG between cells, it will be identified as putative pairwise shared NBG pair.

I applied my previously validated pairwise interaction methods in Section 3.2.4 on analyzing thousands of neurons in seven visual areas. ($N_{cells} = 17435$). I analyzed putative shared NBG input between areas (Table 1. and Figure 11.A) and putative functional excitatory/inhibitory interaction. (Table 2. and Figure 6 A, B) I found NBG pairs between LGN, V1 and HVAs as well as within LGN and V1. This confirms at least in few cells in HVA exhibits NBG in their activity. (Table 1.)

Table 1. Number of cells and NBG pairs within/between visual areas. (N_{cell} = 17435, N_{mouse} = $N_{recording}$= 58)

A Number of cells in visual areas across all recordings

V1	LM	RL	AL	PM	AM	LGN	Total
3694	2075	2567	3036	1798	2959	1309	17435

B Number of NBG pairs between visual areas across all recordings

	V1	LM	RL	AL	PM	AM	LGN
V1	149	11	51	30	1	30	745
LM		0	0	0	0	0	31
RL			12	4	1	4	124
AL				1	0	2	54
PM					0	0	6
AM						2	23
LGN							2180

Table 2. Number of time-lagged functional connectivity (TLFC) pairs between visual areas. (N_{cell} = 17435, N_{mouse} = $N_{recording}$= 58)

A Number of Excitatory TLFC between areas across all recordings

Pre \ Post	V1	LM	RL	AL	PM	AM	LGN
V1	1644	12	7	5	10	8	0
LM	6	599	9	42	10	12	2
RL	1	6	654	7	4	14	0
AL	3	24	4	1102	8	24	0
PM	6	3	0	0	587	40	2
AM	0	5	5	5	22	988	4
LGN	33	1	12	2	1	13	365

B Number of inhibitory TLFC between areas across all recordings

Pre \ Post	V1	LM	RL	AL	PM	AM	LGN
V1	1330						
LM		512		15			
RL			549				
AL		13		969			
PM					571	18	
AM					20	760	
LGN							54

5.2.2.1.2 Spectral narrowband gamma power of raw population activity suggests possibility of NBG exist in higher visual areal population activity.

Next, I inspected if NBG exists in population activity in HVA. I looked at the raw LFP of HVA recordings (about 3 hours long) to get power spectral density. I compared spectral power of LFP with the smoothened spectral power, the baseline indicates when there is no NBG (1/f), (Saleem et al., 2017) to verify the existence of residual NBG power.

V1 layer 4 LFP always had a prominent residual NBG power. Among 14 recordings, I found every HVA had residual NBG power at least one recording but not in every recording. ($N_{session} = 15$). Figure 13. shows example power spectral density of different visuo-cortical areas.

5.2.2.2 Narrowband gamma oscillation in HVA population activity is coherent with narrowband gamma oscillation in LGN spiking activity.

Here I tested if NBG in HVA population activity exists across all recording and is coherent with NBG in LGN spiking activity. I used two methods to amplify NBG signal in HVA and verify spike-LFP coherence of the oscillation: spike triggered LFP and cycle histogram. These two analyses are complementary to each other. STLFP shows dominant frequency and power of spike locked oscillations in LFP and cycle histogram focuses on the level of coherence of the specific narrowband between spikes and LFP.

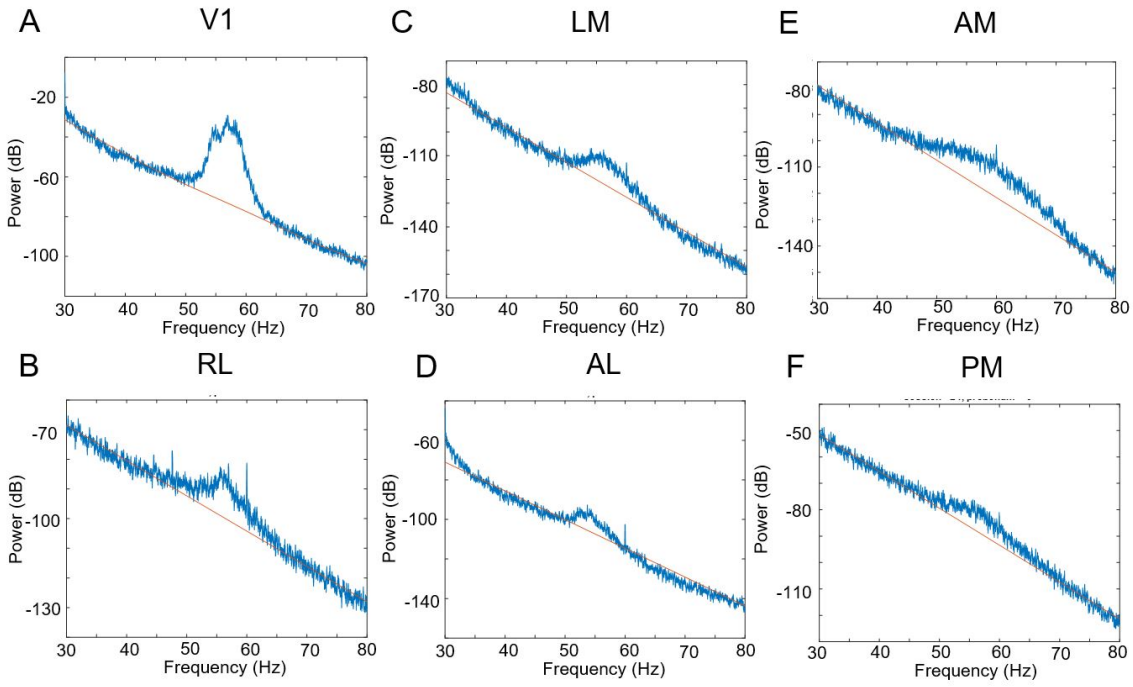

Figure 13. Raw LFP in V1 and higher cortical areas show narrowband gamma oscillation. (each example with one recording)

A. Example spectral power of raw V1 layer 4 LFP of example recording (recording duration = 3hours) that shows clear residual NBG power. (blue) and 1/f smoothened power line as a reference. (red) `

B. Example spectral power of raw RL LFP of example session. Unlike V1 which every recording session had prominent NBG power of raw LFP, only few recordings had prominent NBG power of raw LFP.

C. Same as B but LM LFP.

D. Same as B but AL LFP.

E. Same as B but AM LFP.

F. Same as B but PM LFP.

5.2.2.2.1 Spike triggered local field potential (STLFP) shows reliable narrowband gamma oscillation in HVA

I analyzed spike triggered LFP of cortical areas to see if there is spike driven oscillatory activity in HVA. If there is precise frequency and phase relationship between spiking activity and LFP, STLFP should reveal a clear oscillation. To separate effects that are driven by stimulus, I only used spikes that are not during stimulus presentation (spontaneous activity).

I computed STLFP using spiking activity of identified NBG cells in LGN, and using earliest sink layer of HVA LFP. After I got result STLFP (example using V1 layer 4 LFP, Figure 14.A), I applied spectral analysis to find the dominant frequency of the oscillation and compared with the smoothened spectral power (1/f) to find residual NBG power.

The result of STLFP in every HVA had residual NBG power and the residual power within the NBG band was higher than residual power within BBG band (control). (Figure 14.B, C) This results reassures that the NBG exists in HVA as well and is coherent with LGN spiking activity.

To get a sense of how precise phase coherence is required to exhibit prominent NBG in STLFP, I added uniformly distributed noise to the spike times of LGN spikes. (Figure 17.) With small width of the noise ($\leq$ 4ms, quarter of NBG period), NBG is still prominent. However, larger than 4ms width noise gets rid of NBG.

5.2.2.2.2 Cycle histogram shows clear coherence between HVA LFP and LGN spikes.

If there is phase coherence between spike and LFP, cycle histogram should exhibit one period of phase shifted cosine. Therefore, I extracted the amplitude of cosine from normalized histogram to verify and quantify coherence between spike and LFP (Figure 15.A), and I computed SNR (Figure 15.C) to quantify how strong the coherence is.

The cycle histogram of every HVA LFP exhibited higher coherence than the baseline null hypothesis. (cycle histogram using simultaneously recorded hippocampal LFP). (Figure 15.B, D) As well as result from STLFP, this result reassures that the NBG exists in HVA as well, and is highly coherent with LGN spiking activity.

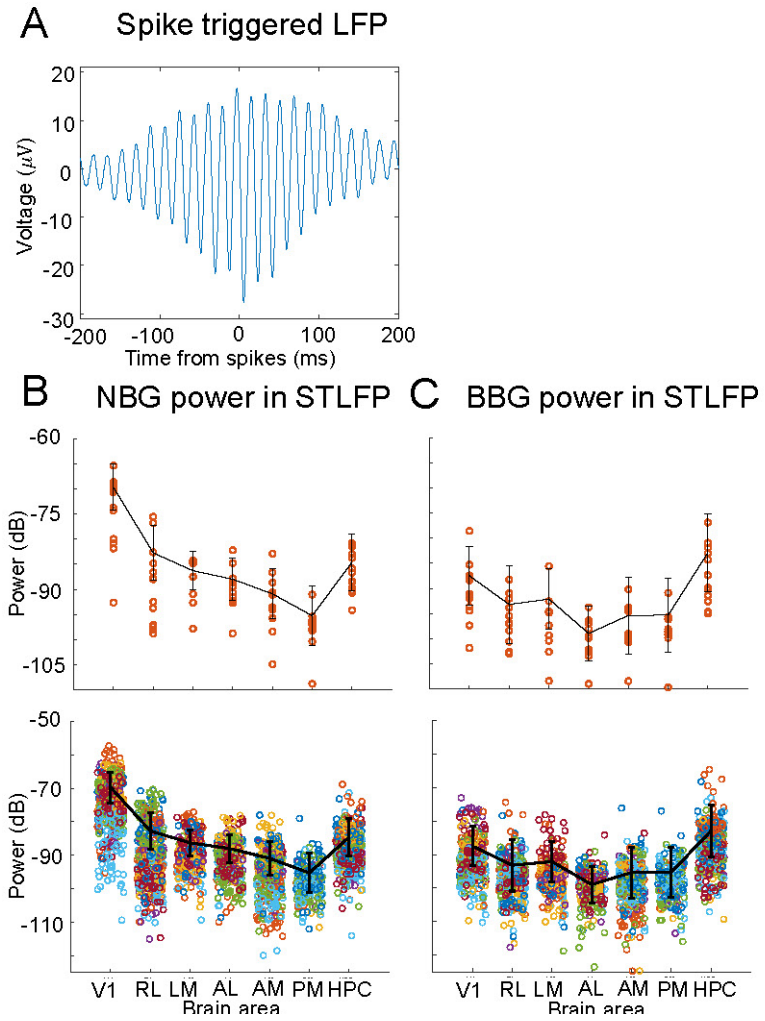

Figure 14. Hierarchy of the power of narrowband gamma oscillation in population activity of visuo-cortical areas revealed with spike-triggered LFP is consistent with the functional hierarchy. (N_{cell} = 402, N_{mouse} = $N_{recording}$= 15)

A. Example STLFP acquired with spikes from an example "narrowband gamma" cell in LGN and V1 LFP.

B. (top) Population average of the NBG power of STLFP of different visuo-cortical areas using "narrowband gamma cell" in LGN of all recording. (red line, standard deviation) Data point means average NBG power of STLFP of each session. (bottom) Same as top. Data point means NBG power of STLFP with each cell. Difference color denotes different recording session.

C. Same as B but BBG power of STLFP as a control.

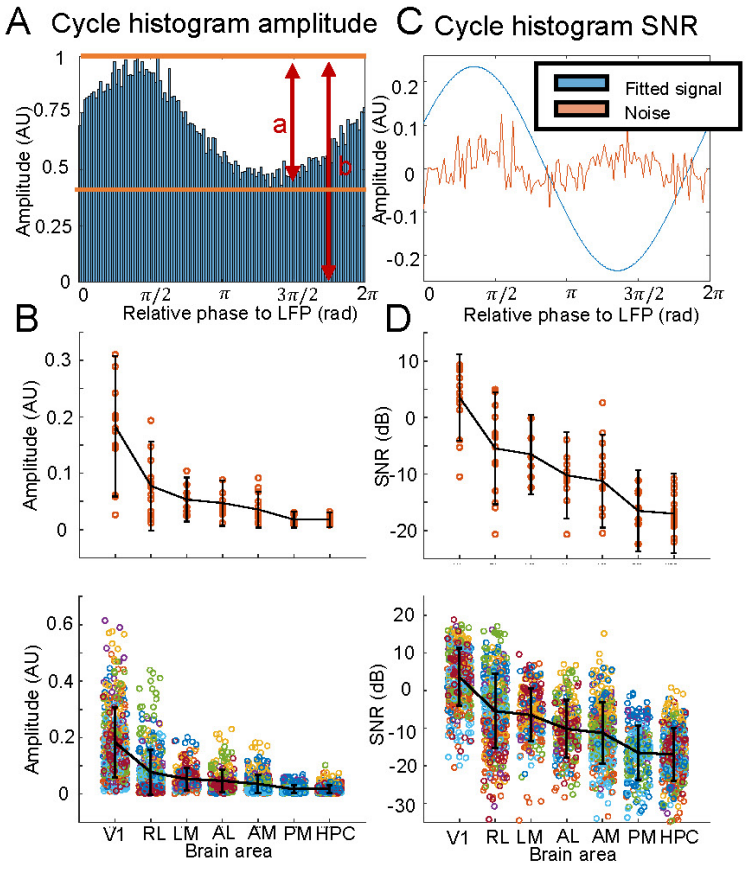

Figure 15. Hierarchy of power of narrowband gamma oscillation in population activity of visuo-cortical areas revealed with cycle histogram is consistent with the functional hierarchy. (N_{cell} = 402, N_{mouse} = $N_{recording}$= 15)

A. Example of signal amplitude from cycle histogram. (a/b) Cosine was fit to the normalized histogram to get the strength of oscillation. Example with V1 LFP and spikes from an example "narrowband gamma" cell in LGN.

B. (top) Population average of cycle histogram amplitude of different visuo-cortical areas using "narrowband gamma cell" in LGN of all recording session. (red line, standard deviation) Data point means mean cycle histogram amplitude of each session. (bottom) Same as top. Data point means cycle histogram amplitude with each cell. Difference color denotes different recordings.

C. Example of signal-to-noise ratio (SNR) from cycle histogram. Signal is the fitted cosine, and noise is the residual normalized to have mean of 0.

D. Same as B but SNR from cycle histogram.

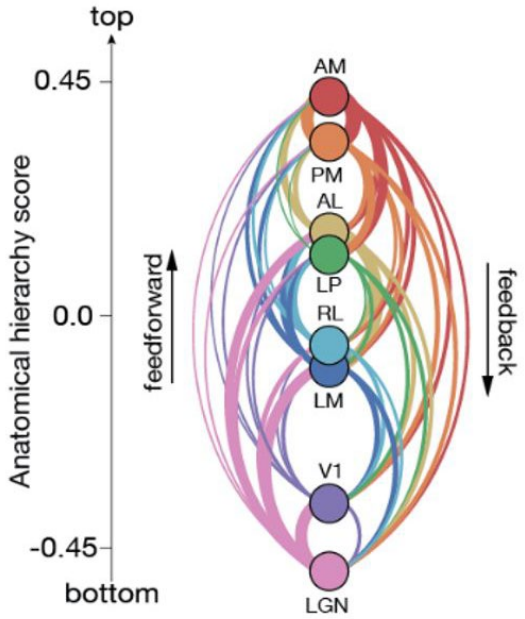

Figure 16. Functional hierarchy is consistent with anatomical hierarchy, from Figure 3 of (Siegle et al., 2019). Functional hierarchy is consistent with anatomical hierarchy from (Harris et al., 2019). Functional hierarchy is revealed with stimulus response properties of each visual areas.

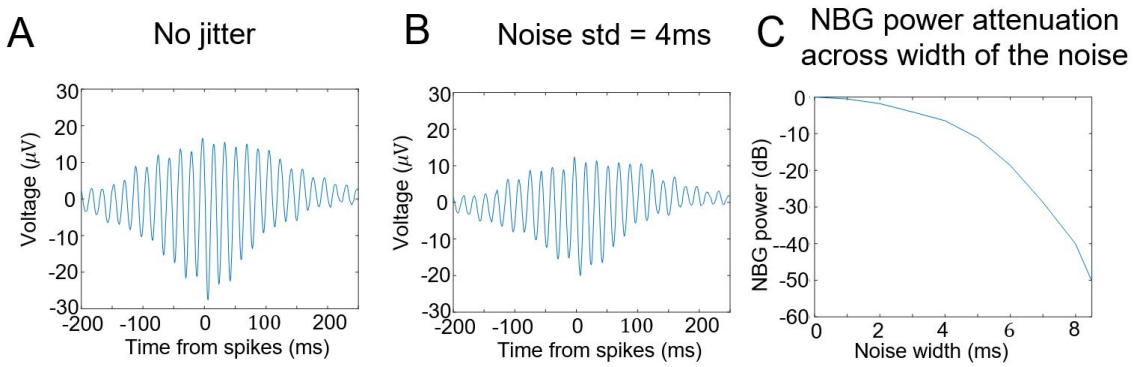

Figure 17. Uniform Jitter on spike times gets rid of narrowband gamma oscillation in spike-triggered LFP. (example with one cell in one recording)

A. Example STLFP without artificial noise on the spike-train.

B. Example STLFP with uniformly distributed noise [-4ms, 4ms] on the spike-train.

C. Attenuation of NBG power with uniformly distributed noise relative to no NBG without noise in example LGN cell and example V1 LFP.

5.2.2.3 The level of coherence and power of NBG across HVA is consistent with anatomical and functional hierarchy from previously reported literatures.

From the spike-LFP coherence analysis from above, I found that the NBG exists in HVA and is highly coherent with LGN spiking activity. Next, I asked if there is any difference between HVAs exhibiting NBG. Interestingly, I found the hierarchy in NBG coherence and power among HVAs all consistently with cycle histogram amplitude, SNR and STLFP NBG power. (V1 > RL > LM > AL >AM > PM). (Figure 14, 15,16. HPC and STLFP BBG power for a control)

Notably, NBG hierarchy among HVAs is remarkably consistent with the previously suggested anatomical hierarchy of the visuo-cortical area found with anatomical tracer experiments (Harris et al., 2019, Figure 5.8.A). Also, the result is consistent with the functional hierarchy found with stimulus response latency, size of receptive field, modulation index, and autocorrelation timescale. (Siegle et al., 2019, Figure 5.8.B)

5.2.3 Discussion

To answer the first question, does NBG exist in higher visual areas, I found NBG exists in HVAs in multiple analysis methods. With spike-spike correlation analysis between cells in different areas, I found single units in HVA that exhibits NBG and correlated with NBG in LGN and V1. Then, I computed the power spectral density of the input layer of different visuo-cortical areal raw population activity. This suggested that there is NBG in population activity of HVA as well as V1, but the raw LFP activity did not confirm that it exists in every recording in every mouse.

Hence, I used spikes from identified NBG cells in LGN to perform spike-LFP coherence analysis. The result of coherence analysis confirmed that there is reliable NBG signal in HVA that is coherent with NBG in LGN spiking activity. Impressively, the power and the level of coherence of NBG in HVA varied across areas, and resembled the anatomical and functional hierarchy suggested from (Harris et al., 2019; Siegle et al., 2019).

This hierarchical representation of NBG in HVA suggests the possibility of NBG is propagated along the same route as visual information is propagated from LGN to HVAs. Moreover, if the possibility is true, it invigorates both of the hypothesis of NBG role: NBG improves visual information processing and NBG itself is a visual information that is encoding luminance.

5.3 How does NBG propagate?

5.3.1 Introduction

With the spike-LFP coherence analysis performed in the previous section, I concluded that there is coherent NBG between LGN and visuo-cortical areas. Next, I asked how coherent NBG is propagated from LGN to multiple visuo-cortical areas through specific subnetworks of neurons, and through specific routs (directly from LGN, or relayed via V1).

First, I asked if NBG propagates through cells in visual areas globally or through subset of cells that exhibits NBG. I answered by comparing the probability of functional connectivity among all cells in visual areas, versus pairs of cells that exhibit NBG.

Additionally, I asked in which route would NBG propagate from LGN to higher visual areas. Since NBG hierarchy is consistent with anatomical and functional hierarchy, my hypothesis is that NBG in HVA is propagated through V1 not directly from LGN. However, the existence of the anatomical (Bienkowski et al., 2019), functional connectivity (Table 2) and NBG pairs (Table 1. and Figure 11) between LGN and HVA, made me want to investigate the route.

5.3.2 Methods

5.3.2.1 Conditional granger causality to reveal NBG propagation from LGN to HVA models

Granger causality is a way to reveal causality between different time series signals by modeling auto-regressive models. (Ding et al., 2006; Stokes and Purdon, 2017) Granger causality is a powerful tool that could estimate causality without performing perturbation experiment. There are several assumptions that Granger causality makes, such the system that generates signal should be linear, time invariant, and stationary. (Ding et al., 2006; Stokes and Purdon, 2017)

For example, in bivariate time series X, Y, the method finds causality by comparing the explained variance of two models:

$$(1)\ X_t = \sum_{j=1}^{\infty} a_j X_{t-j} + \epsilon_t, \qquad var(\epsilon_t) = \Sigma$$

$$(2)\ X_t = \sum_{j=1}^{\infty} b_j X_{t-j} + \sum_{j=1}^{\infty} c_j Y_{t-j} + \eta_t,\ var(\eta_t) = \Gamma$$

$$(3)\ F_{X->Y} = ln\frac{\Sigma}{\Gamma}$$

If Σ is smaller than Γ, Y_{t-j} helps explaining X_t. Hence, there is a causality from X to Y ($F_{X->Y} > 0$).

Granger causality could also be analyzed in the spectral domain, which formulates the coherence and causality of two signals, and identify in which frequency band the causality occurs. (Detailed method in (Ding et al., 2006))

In tri-variate granger causality, between X, Y, Z, it is possible to compute granger causality from X to Y given Z. ($F_{X->Y|Z}$), which could be analyzed in spectral domain as well as in time domain. (Granger-Geweke causality, detailed method in (Ding et al., 2006))

5.3.3 Results

5.3.3.1 NBG is propagated through subnetworks.

I asked if NBG propagates through cells in visual areas globally or through subset of cells that themselves exhibit NBG. To answer this question, I analyzed if the probability of finding functional connectivity increases among identified NBG cells across visual thalamo-cortical areas. I assumed all identified NBG cells from visual areas are from one source oscillation.

5.3.3.1.1 Probability of functional connectivity increases with narrowband gamma oscillation

Interestingly, I found the probability of having functional connectivity increases significantly among identified NBG cells. The probability of having time-lagged-functional-connectivity (TLFC) between cells in LGN and V1 increased more than 10x. (P(TLFC) = 0.04% while P(TLFC|NBG) = 0.55%, Figure 18.A, Table 3.) Surprisingly, I found among LGN and HVA, the probability increased more than 100x with NBG. (P(TLFC) = 0.01 while P(TLFC|NBG = 1.04%, Figure 18.B, Table 3.). Between other areas and time-synced-functional-connectivity (TSFC) showed large increase of probability among identified NBG cells as well. (Detailed result in Table 3, 4.)

However, it is found that the probability of detecting functional connectivity increases with high firing rate of cells. (De La Rocha et al., 2007) Actually, I found that the average firing rate of identified NBG cells were significantly higher than the average

firing rate of all cells. Hence, I performed control analysis where I controlled for the effects of firing rate on detection of correlations.

$(FR_{LGN,NBG} = 13.11\ spikes/s\ (N_{cell} = 1112), FR_{LGN,all} = 11.00\ spikes/s\ (N_{cell} = 1304), FR_{cortex,NBG} = 14.31\ spikes/s\ (N_{cell} = 713),\ FR_{cortex,all} = 5.92\ spikes/s\ (N_{cell} = 16121))$

5.3.3.1.2 Control: probability of functional connectivity given high firing rate cells

Here, I conducted control analysis to rule out the effect of high firing rates contributing to high probability of functional connectivity. I sub-selected cells that are not identified NBG cells in LGN, V1 and HVA that had higher firing rates than the threshold, which matches the average firing rates with the average firing rate of NBG cells.

As expected, the probability of functional connectivity between high firing rates cells were significantly higher than probability with cells that includes low firing rate cells. (significance not shown, Table 3.B and Table 4.B) However, probability of functional connectivity with NBG cells between LGN and visuo-cortical areas, and within/between visuo-cortical areas were significantly higher than that of high firing rate cells. (Table 3, 4) I calculated the significance with binomial t-test using probability of functional connectivity among non-NBG and high firing rate cells as a null probability. (Detailed significance in Table 3.C and Table 4.C) These results suggest that the effect of NBG increasing functional connectivity is not only consequence of having high firing rates but also suggests functional connectivity between NBG cells is actually significantly denser than global functional connectivity.

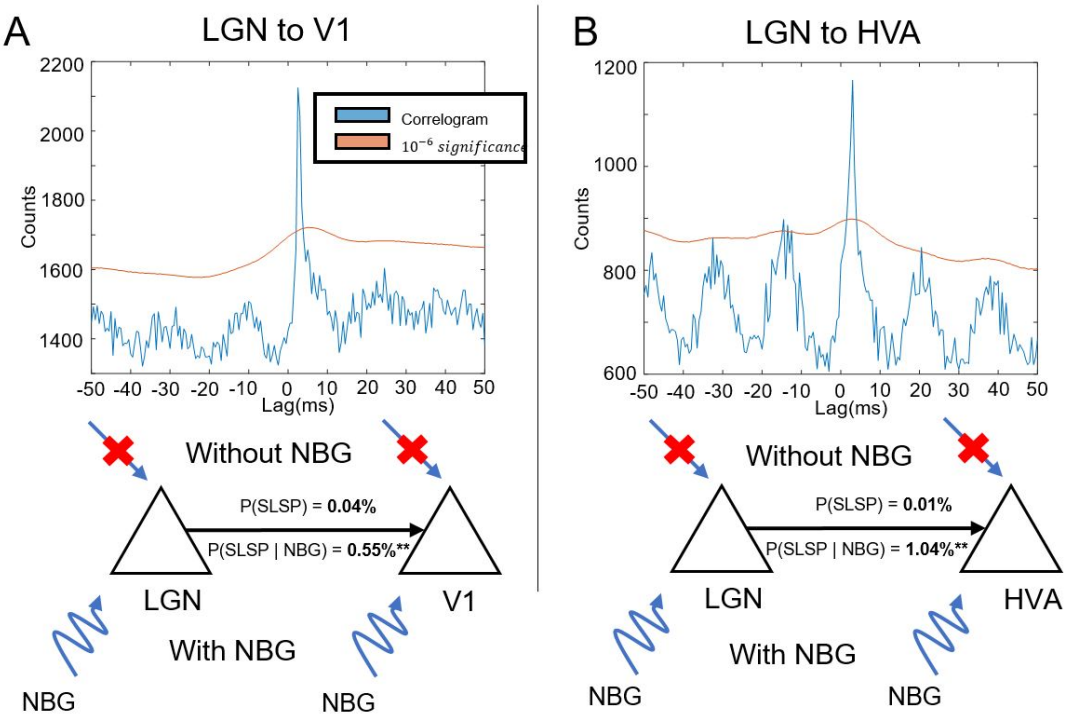

Figure 18. Narrowband gamma oscillation promotes functional connectivity between cells (N_{cell} = 17435, N_{mouse} = $N_{recording}$= 58)

A. (top) Example cross-correlogram of two "narrowband gamma" cells each from LGN and V1. (bottom) Probability of finding time-lagged functional connectivity between all LGN cells and V1 cells is 0.04%. When both cells are identified as "narrowband gamma" cells, the probability increase to 0.55%. (Binomial t-test p < 1e-15)

B. (top) Example cross-correlogram of two "narrowband gamma" cells each from LGN and HVA. (bottom) Probability of finding time-lagged functional connectivity between all LGN cells and HVA cells is 0.01%. When both cells are identified as "narrowband gamma" cells, the probability increase to 1.04%. (Binomial t-test p < 1e-17)

Table 3. Probability of time-lagged functional connectivity is increased among "narrowband gamma" cells (N_{cell} = 17435, N_{mouse} = $N_{recording}$= 58)

A P(TLFC)

	LGN	V1	HVA
LGN	0.56% (419/75148)	0.04% (33/82588)	0.01% (29/249850)
V1	0% (0/82588)	1.09% (2974/273102)	0.005% (42/816200)
HVA	0.003% (8/249850)	0.002% (16/816200)	Within: 0.83% (7271/869708) Inter: 0.015% (310/2076920)

B P(TLFC |High FR & ~ NBG)

	LGN	V1	HVA
LGN	0.73% (157/21476)	0.03% (3/9248)	0.02% (6/29960)
V1	0% (0/9248)	3.51% (542/15398)	0.005% (2/41984)
HVA	0% (0/29960)	0.002% (1/41984)	Within: 3.16% (1228/38762) Inter: 0.06% (57/96204)

C P(TLFC |NBG)

	LGN	V1	HVA
LGN	0.57% (43/7542) P = 0.014	0.55% (16/2892) p = 6.49e-15	1.04% (12/1147) P = 3.39e-17
V1	0% (0/2892)	5.11% (65/1270) P= 7.57e-4	0% (0/440)
HVA	0% (0/1147)	0.68% (3/440) P = 1.893e-7	Within: 1.89% (4/212) p =0.11 Inter: 1.43% (1/70) P = 0.04

Table 4. Probability of time-synced functional connectivity is increased among "narrowband gamma" cells (N_{cell} = 17435, N_{mouse} = $N_{recording}$= 58)

A P(TSFC)

	LGN	V1	HVA
LGN	6.405 (2404/37574)	0.034% (28/82588)	0.024% (59/249850)
V1	0.034% (28/82588)	4.916% (6711/136551)	0.0261% (213/816200)
HVA	0.024% (59/249850)	0.0261% (816200)	Within: 2.736% (11988/434864) Inter: 0.051% (533/1038460)

B P(TSFC | High FR & ~ NBG)

	LGN	V1	HVA
LGN	8.35% (897/10738)	0.14% (13/9248)	0.08% (23/29960)
V1	0.14% (13/9248)	30.65% (2360/7699)	0.20% (86/41984)
HVA	0.08% (23/29960)	0.20% (86/41984)	Within: 19.99% (3874/19381) Inter: 0.27% (263/96204)

C P(TSFC | NBG)

	LGN	V1	HVA
LGN	13.02% (491/3771) P <1e-20	0.48% (14/2892) P = 6.53e-5	0.26% (3/1147) P = 0.05
V1	0.48% (14/2892)	36.85% (234/635) P = 1.27e-4	0.23% (1/440) P = 0.36
HVA	0.26% (3/1147)	0.23% (1/440)	Within: 21.70% (23/106) P =0.085 Inter: 4.29% (3/70) P = 9.31e-4

5.3.3.2 Result identifying signal propagation route from LGN to HVA is obscure

To answer how NBG propagates from LGN to HVA, I performed granger causality analysis on LGN, V1 and RL time series signal during spontaneous activity. I used V1 and RL population activity (LFP), and LGN multi-unit activity of identified NBG cells. I used LGN multi-unit activity instead of LFP because mouse LGN does not exhibit laminar structure or recurrent excitatory connections, so low frequency component of extracellular recording does not represent synchronized excitatory population activity. (Buzsaki et al., 2012)

To start with, I analysed bivariate Granger causality between two areas. Between, V1 and RL LFP, there was significant causality in NBG band. The causality was bidirectional that V1 to RL had higher causality than RL to V1. ($F_{V1->RL}(NBG) = 0.2, F_{V1->RL}(NBG) = 0.13$) However, between LGN multi-unit and both V1 & RL LFP, I also found significant causality from cortical area to LGN. ($F_{V1->LGN}(NBG) = 0.2, F_{LGN->V1}(NBG) = 0.07$) This result conflicts with result from existing literature that did optogenetic perturbation experiment and found NBG in V1 comes from LGN. (Saleem et al., 2017)

There were a lot of uncontrolled variables in the analysis, such as LGN uses multi-unit activity, and V1 & RL uses LFP, uncertain cause of difference in result on generative data. Hence, the result using tri-variate Granger causality, $F_{LGN->RL|V1}(NBG)$ was also not interpretable.

5.3.4 Discussion

To answer the question how does NBG propagates, I asked two sub-questions:

1. Does NBG propagate through subnetwork or global network?
2. In which route does NBG propagate from LGN to HVA?

For the first question, I compared the probability of functional connectivity between every cell and identified cells. Due to the limitation of method, I identified only cells that exhibits strong NBG. Hence, it is still possible that every cell exhibits NBG. If it is the case, the probability of functional connectivity should not increase among NBG cells. However, I found the probability is significantly higher with identified NBG cells than it with every cell. This result gets rid of the possibility that NBG is expressed in every cell in the area. Hence, I conclude that NBG is expressed only subset of cells in visual thalamo-cortical areas, and propagate through subnetwork.

I assumed if all identified NBG cells from visual areas are from one subnetwork. Hence, I treated all identified NBG cells equally. However, it is still possible that there is more than one subnetwork and produced the result I observed. If I was able to find cells within each subnetwork and did the same analysis, the effect increases probability of functional connectivity could be larger. However, this analysis is strongly limited by the number of potential functional connectivity because the odds of detecting functional connectivity between cells are very low, especially between areas. Hence, having multiple conditions on probability would make the analysis non-interpretable due to lack of statistical power.

For the second question, how NBG propagate from LGN to HVA, I did not get a meaningful result. These could be due to multiple reasons.

1. The inconsistency of the type of time-series signal (LFP for cortical areas, spike-train for LGN) in the brain could affect the result.
2. The assumption of linear, time-invariant and stationary could be wrong.
3. Granger causality is not an appropriate method on this problem.

Therefore, identifying which route NBG propagate from LGN to HVA remains unresolved question. However, the result from previous section that the level of NBG power and coherence in HVA is consistent with anatomical and functional hierarchy, suggests that NBG in LGN goes to HVA through V1 as a more dominant pathway. If NBG in LGN directly propagates to HVA not through V1, I should see higher power or higher coherence in some HVA that is not consistent with anatomical and functional hierarchy.

5.4 What is the role of NBG?

The role of neural oscillations has been mysterious for decades. (Buzsaki and Draguhn, 2004; Fries, 2005, 2009, 2015) There are several hypothesis about neural oscillation, but there is still on-going active debate on its role. The most fundamental discussion is if neural oscillation is a by-product of neuronal periodic synchronization (provoking oscillation artificially would not benefit neural information processing), or if nature evolved with a specific information transmission purpose. (provoking oscillation artificially would benefit neural information processing) (Buzsaki and Draguhn, 2004) I investigated potential contribution of NBG on neural processing without assuming one of the hypotheses.

(Saleem et al., 2017; Storchi et al., 2017) reported that NBG in LGN is coherent across cells. In addition, (Storchi et al., 2017) found that coherence of the oscillation is more prominent during higher luminance. As done in these literatures, I also hypothesized the coherence among neurons is a key clue in inspecting the role of the NBG. Hence, I first analyze NBG coherence among identified NBG cells in LGN, and suggest two hypotheses based on the result of coherence and findings from previous sections.

5.4.1 Is NBG phase coherent across cells in LGN?

In this section, I analyzed coherence of NBG among identified NBG cells to check if I see the same thing with the Allen Institute dataset.

5.4.1.1 Methods

5.4.1.1.1 Phase of oscillation in cross-correlogram

Among cross-correlogram that shows clear oscillation, I computed the phase of the oscillation at 0ms lag. (Figure 19.A, B) First, I bandpass filtered the cross-correlogram to a band of interest. Then, I Hilbert transformed the bandpass filtered signal, to get instantaneous phase at 0ms lag.

5.4.1.1.2 Phase of oscillation in cycle histogram

I computed cycle histogram and fitted a cosine. (Figure 20.A, B, C) The fitted cosine has phase offset and it is used as a phase of an oscillation.

5.4.1.2 Results

5.4.1.2.1 Narrowband gamma phase of LGN cells using cross-correlogram shows two distinct clusters in NBG phase.

Among identified NBG cells in LGN I sub-selected cells that visibly had high NBG power in its auto-correlogram. ($N_{session} = 1, N_{cell} = 17$.) To test coherence of NBG among these cells, I computed cross-correlogram between these cells and one NBG cell outside of the thalamus, V1 layer 4 that had prominently high NBG power. I found there are two groups of cells in LGN that have different NBG phase. (Figure 19.) One cluster of cells had near 0 phase offset, so I named them "coherent cluster", and the other cluster had near $\pi/2$ phase off, so I named them "phase OFF cluster". ($N_{cell,coherent} = 7, N_{cell,phase\ off} = 10$)

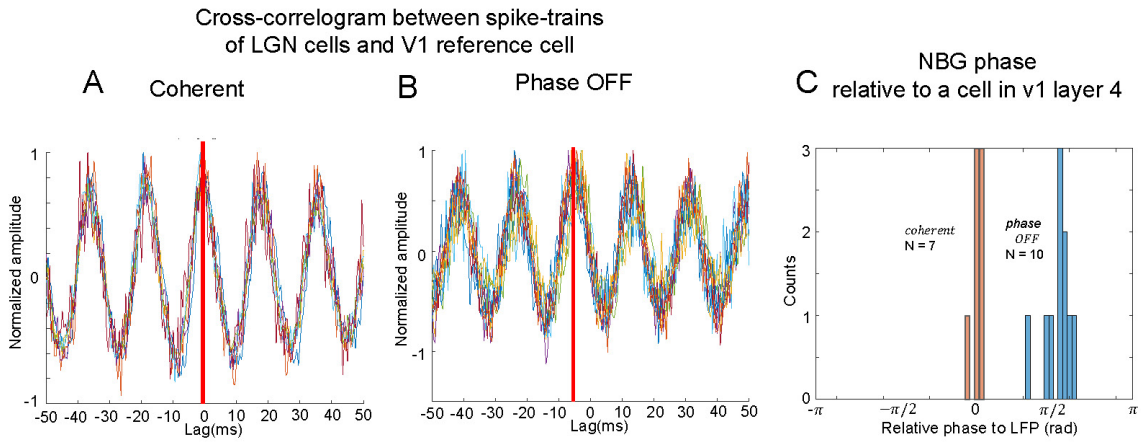

Figure 19. There is two distinct NBG phase cluster reference on V1 spiking activity using cross-correlation. (N_{cell} = 17, N_{mouse} = $N_{recording}$= 1)

A. Example cross-correlogram of cells in LGN that strongly exhibit NBG in its auto-correlogram (I call them "coherent cluster", subset of "narrowband gamma" cells) and reference cell in V1 layer 4 that exhibits NBG in example session. All cross-correlograms exhibits coherent NBG. Phase acquired with Hilbert transform is around 0 at 0ms lag. (N_{cell} = 7)

B. Cross-correlogram between cells from "phase OFF cluster" and V1 reference cell. Phase acquired with Hilbert transform is around $\pi/2$ at 0ms lag. (N_{cell} = 10)

C. Histogram of NBG phase of cells in LGN that strongly exhibiting NBG reference on reference cell inV1 layer 4. (N_{cell} = 7)

5.4.1.2.2 Relative NBG phase of LGN cells using cycle histogram also shows two clusters clearly.

I asked if this phase cluster is maintained relative to V1 layer 4 population activity. Hence, I computed cycle histogram using these cells with V1 layer 4 LFP. I found another clear clustering effect but on different phase offset with the previous result with cross-correlogram. (Figure 20.)

Hence, I questioned why there is difference in phase offset between referenced on single unit and population activity. To answer, I computed cycle histogram with the V1 layer 4 cell that was used as a reference in the previous analysis. I found that this cell also clusters on the phase where coherent cell phase clusters. (Figure 20. C) This is consistent with the previous literature that showed the trough of gamma oscillation in cortical LFP follows after single unit spiking activities. (Hasenstaub et al., 2005) If I account this effect, I get consistent phase cluster with referencing to single cell in V1 layer 4. (Figure 20.D, E)

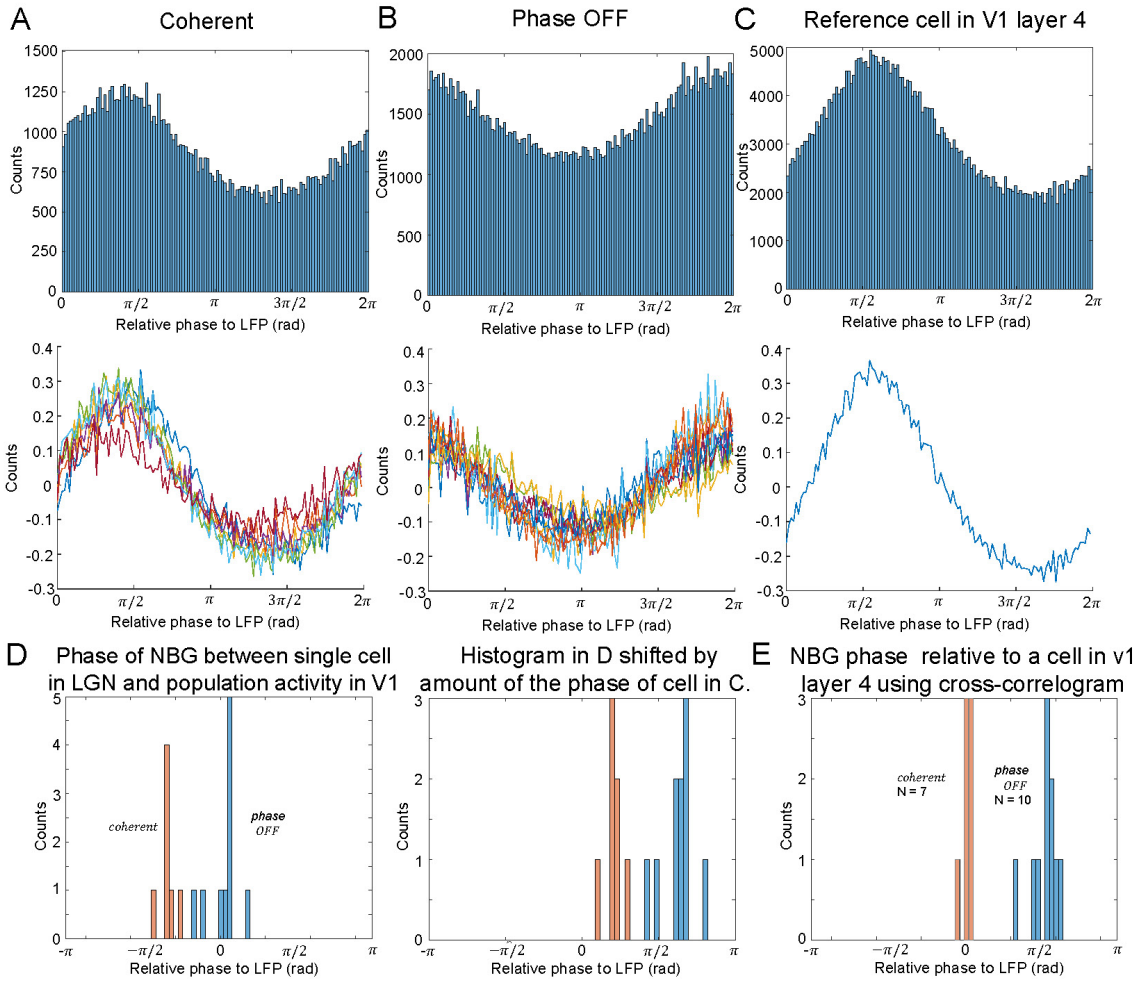

Figure 20. The phase clusters are clear referencing to population activity. (N_{cell} = 17, $N_{mouse} = N_{recording}$= 1)

A. (top)Example cycle histogram using spikes of an example cell from "coherent cluster" in LGN and V1 layer 4 LFP. (bottom) Normalized cycle histograms using spikes of all cells from "coherent cluster" in LGN. (N_{cell} = 7)

B. Same as A but with cells from "phase OFF cluster". (N_{cell} = 10)

C. Same as A but with the reference cell inV1 layer 4 from the previous analysis. (same cell from Figure 19).

D. (left) Histogram of NBG phase using cycle histogram. (N_{cell} = 17) (right) Histogram shifted by the phase of the reference cell in V1 layer 4 shown in C.

E. Same figure from Figure 19. C.

5.4.1.2.3 Phase cluster is maintained throughout the recording.

I checked if this NBG relative phase is maintained across the recording. I split the spike-train to hundred segments of 100s spike-trains and computed NBG phase using cross-correlogram. (Figure 21.) I confirmed that NBG relative phase is maintained across recordings while BBG relative phase is not.

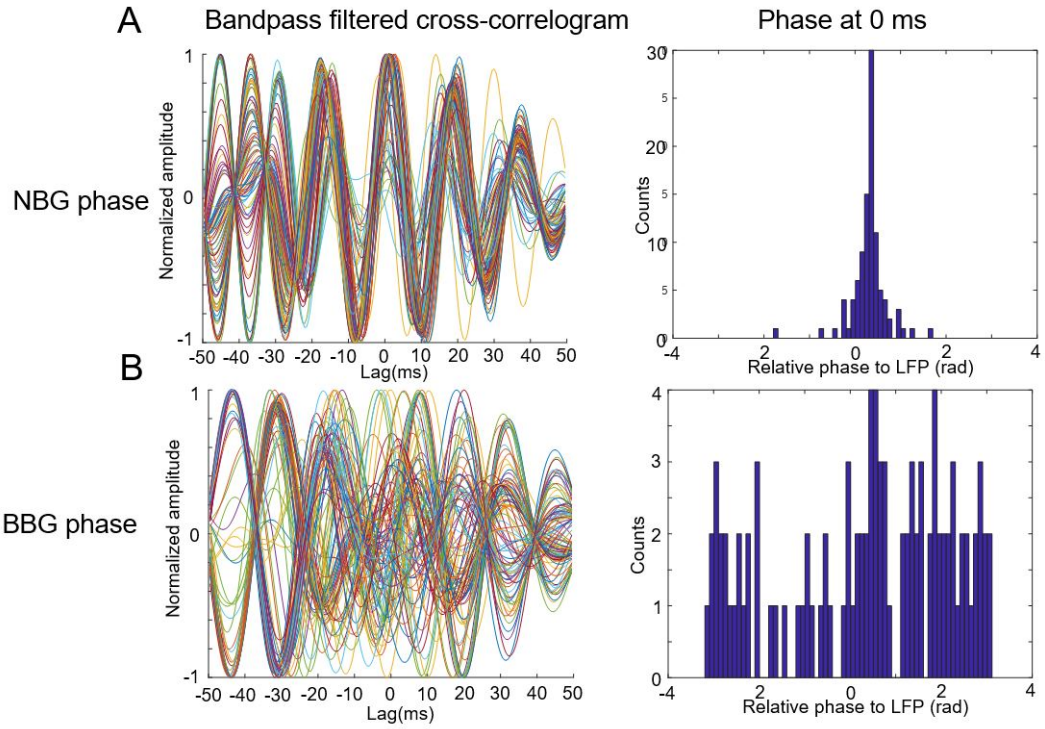

Figure 21. The phase cluster is maintained throughout the recording (example with one cell in one recording)

A. (left) Bandpass filtered (NBG) cross-correlograms between one cell from "coherent cluster" in LGN and the reference cell inV1 layer 4 of 100s of hundred segments. (right) Histogram of NBG phase at 0ms lag of correlogram calculated with Hilbert transform. The phase at 0ms is coherent among segments.

B. Same as A, but bandpass filter to BBG. The phase is not coherent among segments.

5.4.1.2.4 The phase of narrowband gamma oscillation of LGN cell indicates ON/OFF preference.

In the previous result with one example recording, I found that there are two groups of cells that $\pi/2$ phase off of NBG phase relative to V1 layer 4, both for single unit spiking activity and population activity. Here, I tested if this NBG phase cluster denotes different visual preference.

Surprisingly, neurons in each of the two preferred phase clusters also have different visual responses. "Coherent cluster" responds to positive contrast full-field flash stimulus, (ON preference) and "Phase off cluster" responds to negative contrast full-field flash stimulus. (OFF preference). (Data not shown).

I asked if this would be maintained property across different mice. I clustered the identified NBG cells in LGN by its responsive properties to full-field flash stimulus: transient ON/OFF preference cells and ambiguous cells. (Figure 22. A, B. $N_{mouse} = N_{sessions} = 14$, $N_{ON\ pref} = 167$, $N_{OFF\ pref} = 96$)

Then, I computed NBG phase of these cells relative to a single highest NBG power ON preference cell in LGN (previously "coherent cluster"). Remarkably, ON/OFF preference cells had again $\pi/2$ phase offset between them, visibly gaussian distributed. (Figure 22. C). Also, I was able to see clear clustering reference to V1 layer 4 LFP. (Figure 22.D)

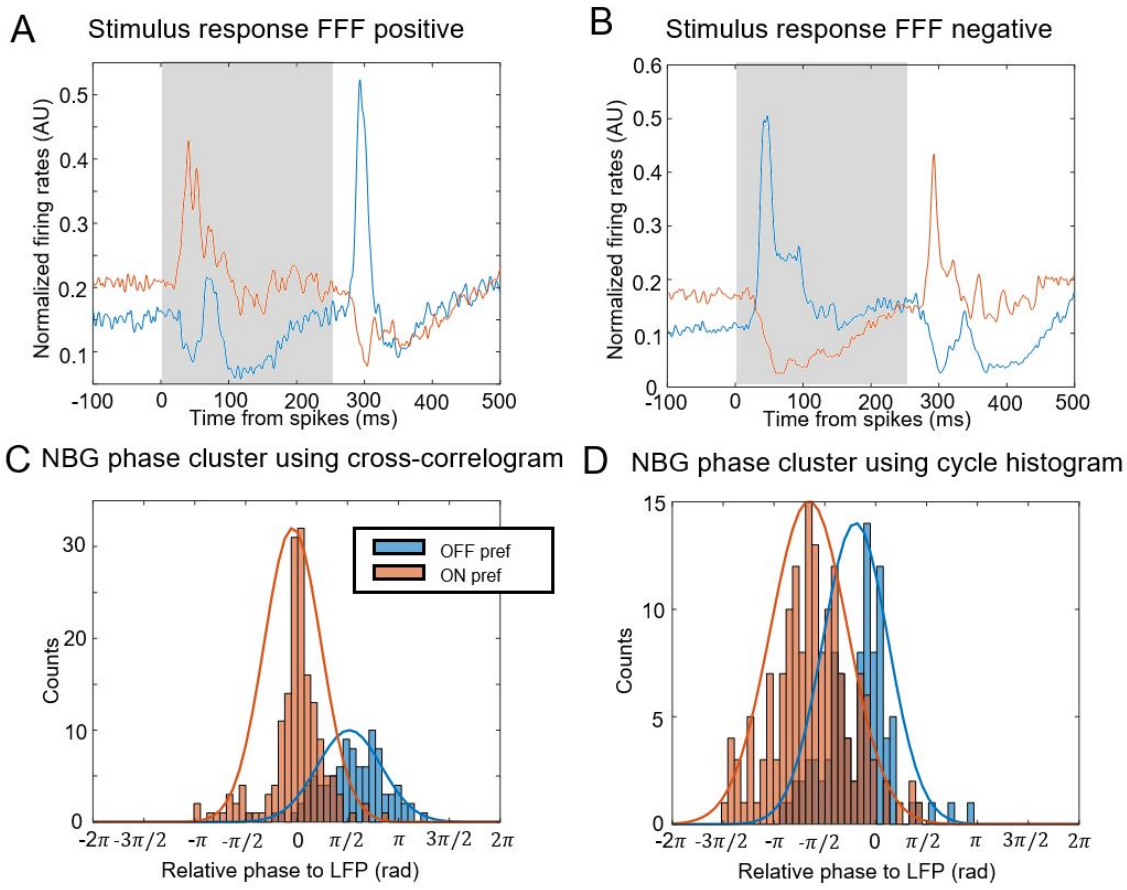

Figure 22. ON/OFF preference cells in LGN locks to different narrowband gamma oscillation phase. ($N_{cell,\ ON\ pref}$ = 167, $N_{cell,\ OFF\ pref}$ = 96, N_{mouse} = $N_{recording}$= 14)

A. Average stimulus response of response of ON preference cells (red) and OFF preference cells (blue) to white full field flash. Color code is maintained within Figure 22.

B. Average stimulus response of response of ON/OFF preference cells to black full field flash.

C. NBG phase of ON preference cells (red) and OFF preference cells (blue) relative to one ON preference cell in LGN identified with pairwise cross-correlogram. Two clusters are clearly separated.

D. Same as A but reference to V1 layer 4 LFP identified with cycle histogram. Two clusters are also clearly separated.

5.4.1.2.5 Phase cluster is maintained to downstream higher visual areas

The benefit of using cycle histogram to get NBG phase is that I could use LFP of different areas as a reference. I computed NBG phase of identified ON/OFF preference NBG cells in LGN reference to different visuo-cortical LFP.

Interestingly, the phase cluster was maintained to downstream higher visual areas. The sensitivity of two clusters decreased with more downstream areas according to the anatomical and functional hierarchy. (Figure 23.A (Harris et al., 2019;Siegle et al., 2019)) The effect primarily comes from the distance of the mean of the cluster than standard deviation of the gaussian fit. (Figure 23.B) As expected from the result about NBG power and coherence across different HVA, PM did not exhibit any clusters while other areas showed clustering effect.

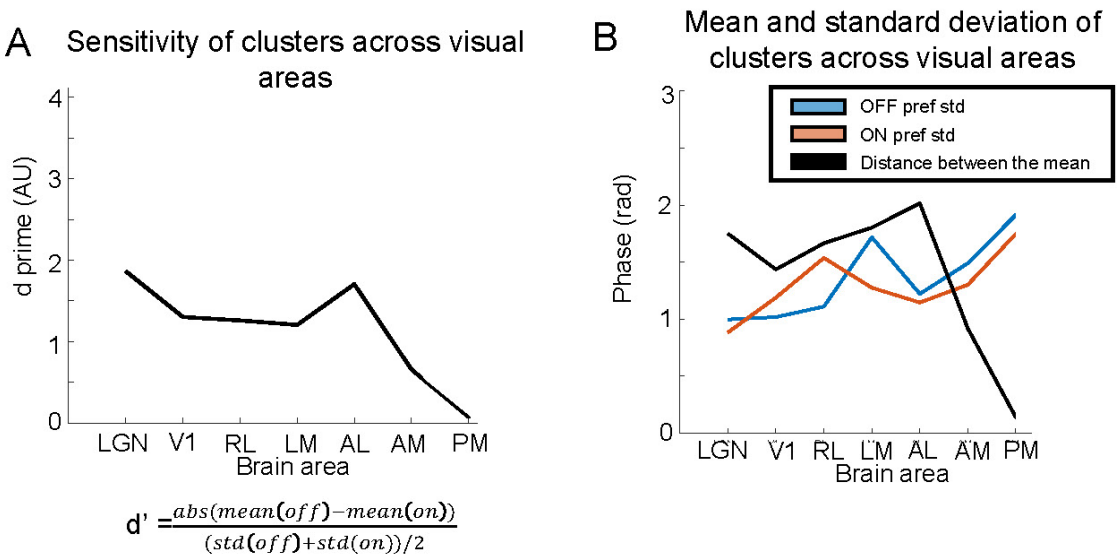

Figure 23. Phase cluster is maintained to downstream higher visual areas. ($N_{cell,\ ON\ pref}$ = 167, $N_{cell,\ OFF\ pref}$ = 96, N_{mouse} = $N_{recording}$= 14)

A. Sensitivity (d prime, defined below the figure.) of two gaussian fit on NBG phase cluster of ON/OFF preference cells reference to different visual areas. (see Figure 22.D for an example) Sensitivity is the highest at the most upstream area, and lowest at the most downstream area which is consistent with functional hierarchy. (One exception with AL)

B. Standard deviation of gaussian fit on narrowband gamma phase cluster of ON preference cells (red) and OFF preference cells (blue) reference to different visual areas.

5.4.2 Discussion

The result of the coherence in spiking activity shows that the phase of neuronal spiking relative to NBG forms two distinct neuron clusters that also have different ON/OFF preferences. This NBG phase cluster is not only limited in LGN and V1 but also propagates to higher order visual areas in mice.

This result is different from what has been shown in previous literatures about NBG, which shows one coherent NBG cluster among LGN cells exhibiting NBG. (Saleem et al., 2017; Storchi et al., 2017) I suspect two reasons for the different result. First, the number of isolated neurons in LGN is significantly larger with the Allen Institute dataset than with datasets used in previous literature. Second, the authors of these previous studies computed the phase relative to the multi-unit spike-train while I computed phase relative to ON preference single-unit spike train. Even though single-unit is usually less general than multi-unit, in this case with two distinct neuronal clusters, phase referencing on single-unit from one specific cluster would have less bias.

A discovery from the previous section that NBG propagates through subnetwork assumes one source oscillation. In contrary, the finding of two distinct neuronal clusters in LGN suggests that there are at least two coherent oscillations is present in LGN and reach to the cortex. I did not analyse how the functional connectivity changes between two neuronal clusters due to the lack of the statistical power with small number of single units.

I performed supplementary analysis to clarify the source of the neuronal cluster by analysing a public dataset containing single units from the optic tract. (Schröder et al., 2020) I found NBG from 9 single units out of 24 total units ($N_{recording}$ = 6) in the optic

tract. I verified that NBG in these units disappears with complete darkness which is consistent with the features of NBG previously found by literatures. (Saleem et al., 2017; Storchi et al., 2017) However, there was no NBG phase offset between ON/OFF preference cells. Due to the lack of the statistical power with 24 units I am not able to conclude, but I suspect that NBG phase offset between the neuronal clusters in LGN is generated in LGN, not inherited from the retina.

I did not find single unit neuronal clusters with NBG phase offset in V1. I anticipate this is primarily because ON/OFF preference single units that has NBG phase offset from thalamus merge at V1. On the other hand, the phase cluster is maintained in the population activity of V1 and downstream higher visual areas. This implies that the two phases of NBGs affect information processing in HVAs as well as in the thalamus.

5.4.3 Suggested hypotheses

With the finding of two distinct neuronal clusters in LGN, and previous findings made in this Chapter, I suggest two hypotheses on the role of NBGs in the visual systems: first, communication through coherence, and second, NBG as a computationally efficient way to encode luminance.

It is found from (Saleem et al., 2017) that the source of NBG in the cortex is LGN. On the other hand, I found that the hierarchy of NBG coherence and power in the visual cortex is consistent with the anatomical (Harris et al., 2019) and functional hierarchy (Siegle et al., 2019) that was identified with anatomical tracer experiments and stimulus

response properties. These two findings imply that NBG propagates from LGN to visuo-cortical areas along the same pathway that a stimulus propagates. In other words, the subnetwork that NBG propagates is likely to be a subset of general stimulus propagation pathway. Hence, I hypothesize that NBG has a role in sensory processing, either by modulating stimulus response or by carrying sensory information.

5.4.3.1 Hypothesis 1: Communication through coherence

Communication through coherence is a major hypothesis that explains the role of the neural oscillation in the brain. (Fries, 2005, 2015) This hypothesis suggests that the neural oscillation synchronizes the excitability of multiple brain areas to help process sensory information. My first hypothesis of the role of NBG is that the NBG synchronizes excitability of retinal-thalamo-cortical pathway and provides a "window of opportunity" for visual information to be propagated.

To verify this hypothesis, I suggest two analyses: first, to investigate if NBG phase affects stimulus response. (Cardin et al., 2009; Siegle et al., 2014) Second, to investigate if synchronized excitability of NBG between visual areas reflects stimulus response latency difference between visual areas (i.e. if NBG phase delay is consistent with stimulus response latency difference between visual areas).

5.4.3.2 Hypothesis 2: Narrowband gamma oscillation encodes luminance in the early visual system

The findings made in this thesis imply that NBG propagates from LGN to visuo-cortical areas along the pathway that a stimulus propagates, which permits the possibility of NBG as a modulator of sensory processing, and itself as a form of visual information.

Other discoveries in this thesis also give clues about the role between the two suggested hypotheses. The result of NBG propagation through subnetworks eliminates the possibility of NBG as a global modulator of visual processing in visual areas. Rather, it modulates specific part of the visual information processing, or itself is a form of visual information.

NBG power increases with the luminance and irradiance. (Saleem et al., 2017; Storchi et al., 2017) Particularly, NBG amplitude in LGN coherent spiking activity revealed with Hilbert transform could recover local chirp stimuli (black and white luminance reversals), but if coherent spiking activity was perturbed with the shuffled trials, the recovery was less clear. (Storchi et al., 2017) This suggests NBG has the ability to encode luminance information.

In addition to the findings that NBG is coherent among single cells in LGN made from (Storchi et al., 2017), I found that ON/OFF preference cells lock to different phases of NBG. Moreover, the phase difference between two clusters is near $\frac{\pi}{2}$ ($N_{recording}$= 14), which makes the oscillation of two types of cells orthogonal.

(Storchi et al., 2017) suggested that luminance information is encoded by instantaneous amplitude of NBG computed with the Hilbert transform. However, the Hilbert transform is non-causal computation and requires long memory, which is not biologically plausible. If there are two orthogonal oscillations, the brain does not need to compute instantaneous amplitude with the Hilbert transform. Hence, with the finding that the oscillations of ON/OFF clusters are orthogonal to one another, I suggest that NBG is a method for encoding luminance information in the early visual systems in a computationally simple and efficient way.

CHAPTER 6. CONCLUSION

This thesis contains a two-stage research project: first, validating the reliability of large-scale neural data analysis through benchmarking two commonly used spike-sorting algorithms, and developing an intrinsic signal imaging (ISI) analysis pipeline that identifies visuo-cortical areas non-invasively. Second, these reliable methods were used in the investigation of coherent neural oscillation in multiple visual brain areas with publicly available large-scale dataset of simultaneous recordings of multiple visual areas – the Allen Institute visual coding dataset. (Siegle et al., 2019)

Large scale electrophysiology presents unprecedented opportunities in investigating how networks and systems of neurons process information. However, problems with spike-sorting remain unresolved, so researchers who use extracellular electrophysiology should always be careful when interpreting spiking data.

In the first chapter of this thesis, I tried to the best of my ability to understand and relay the constraints of the spike-sorting algorithms I use, and that are commonly used in the field. I verified that the fundamental difference in mechanisms in detecting and classifying spikes influences the analysis of scientific questions. The difference in detectability of spikes in high firing backgrounds, with many spatio-temporally overlapping spikes, caused different interpretation of single-unit receptive field statistics and statistical detectability in short latency functional connectivity.

In the second chapter of this thesis, I developed an analysis pipeline of an intrinsic signal imaging (ISI) system. ISI reveals a functional map of the brain non-invasively. As

the fields progress to investigate more complex mechanisms of the brain, experiments have become more complex and costly, which requires training mice to a behavioural task for weeks and simultaneous recording multiple brain areas. Hence, it is necessary to reliably localize the functional brain area, which ISI provides.

I developed an analysis pipeline that identifies the retinotopic map and reveals higher order visual cortical areas (HVAs) of the mouse visual cortex using Fourier analysis. Also, I created the algorithm that aligns two frames of the same object taken with different wavelength: red and green or in a different recording day. This algorithm could be used to align a computed functional map to a visible indicator on the brain, and to merge functional maps from multiple recording days to make a higher quality functional map.

The Fourier analysis method I used (Kalatsky and Stryker, 2003) approximates the response tuning function of each pixel of brain area to a cosine. I suggest that using a higher order approximation of the response tuning function would result in more accurate and efficient analysis methods.

NBGs have never been measured in the visual cortex of mice beyond V1. This is primarily due to the smaller signal, compare to V1 and LGN, but also due to the lack of simultaneous recording ability and appropriate analysis techniques. I used publicly available large-scale neural recording dataset and I applied validated methods to answer questions about the oscillation.

I made several novel discoveries about NBG. First, I found the presence of NBG over multiple visual areas, and the existence of hierarchy in the coherence and the power

of NBG, consistent with functional hierarchy. This suggests that NBG propagates feed-forwardly from LGN to visuo-cortical areas along the pathway that a stimulus propagates.

Second, NBG forms two distinct neuron clusters in the coherence of spiking activity that gives an orthogonal phase relative to one another, and also have different ON/OFF preferences. This NBG phase cluster is not only present in LGN and V1 but also propagates to mouse higher order visual areas (HVAs) through subnetworks, which suggests a local function of NBG in visual processing with two distinct oscillations.

With these discoveries, I suggest two hypotheses: first, that NBG synchronizes the excitability of multiple visual areas to modulate visual processing; and second, that NBG encodes luminance information transmitted from the retina to higher order visual areas in a computationally plausible way. (HVAs) Both of these hypotheses assume that NBG has a role in visual processing and that it can influence visual perception. It is known that NBG promotes detection of visual stimuli (Speed et al., 2019), but how it promotes is still unresolved. The Allen dataset used here lacks behavioural output of an animal which limits the ability to analyse how NBG affects visual perception. However, the findings made in this thesis suggest keys to how NBG affects visual perception.

Moreover, if NBG exists in different species is another important question to be classified. Similar narrowband oscillation within the gamma range was also found in LGN of anesthetized cat that is propagated from the retina. (Koepsell et al., 2009) To the best of my knowledge, NBG have not studied in non-human primates and humans. Identifying if NBG is a specie specific feature, or a general feature of mammal is a remaining important question.

With the development of experimental techniques and behavioural methodology, the capacity of these experiments is growing rapidly. It is possible to train a transgenic animal to a behavioural task for weeks and months, and simultaneously record multiple brain areas while optogenetically perturbing brain areas. (Siegle et al., 2014) This gives exciting opportunity for experimenters to answer interesting questions that could not been answered beforehand.

However, analysing and interpreting this complex experimental data is also becoming increasingly more difficult. Small bias and error in analysis can lead to misleading conclusions, due to both difficulty in controlling many variables as well as neuronal variability that we have not identified yet, which I learned throughout master's thesis project. Hence, I suggest that it is essential to carefully select reliable analysis methods with sufficient validation before applying to experimental datasets.

REFERENCES

Alessio P. Buccino, C.L.H., Jeremy Magland, Samuel Garcia, Joshua H. Siegle, Roger Hurwitz, Matthias H. Hennig (2019). SpikeInterface, a unified framework for spike sorting. In bioRxiv.

Berger, H. (1929). Über das elektroenkephalogramm des menschen. Archiv für psychiatrie und nervenkrankheiten 87, 527-570.

Bienkowski, M.S., Benavidez, N.L., Wu, K., Gou, L., Becerra, M., and Dong, H.W. (2019). Extrastriate connectivity of the mouse dorsal lateral geniculate thalamic nucleus. J Comp Neurol 527, 1419-1442.

Buccino, A.P., Hurwitz, C.L., Magland, J., Garcia, S., Siegle, J.H., Hurwitz, R., and Hennig, M.H. (2019). SpikeInterface, a unified framework for spike sorting. bioRxiv, 796599.

Buzsaki, G. (2004). Large-scale recording of neuronal ensembles. Nat Neurosci 7, 446-451.

Buzsaki, G., Anastassiou, C.A., and Koch, C. (2012). The origin of extracellular fields and currents--EEG, ECoG, LFP and spikes. Nat Rev Neurosci 13, 407-420.

Buzsaki, G., and Draguhn, A. (2004). Neuronal oscillations in cortical networks. Science 304, 1926-1929.

Buzsaki, G., and Wang, X.J. (2012). Mechanisms of gamma oscillations. Annu Rev Neurosci 35, 203-225.

Cardin, J.A., Carlen, M., Meletis, K., Knoblich, U., Zhang, F., Deisseroth, K., Tsai, L.H., and Moore, C.I. (2009). Driving fast-spiking cells induces gamma rhythm and controls sensory responses. Nature 459, 663-667.

Carlson, D., and Carin, L. (2019). Continuing progress of spike sorting in the era of big data. Curr Opin Neurobiol 55, 90-96.

Cohen, M.R., and Kohn, A. (2011). Measuring and interpreting neuronal correlations. Nat Neurosci 14, 811-819.

Das, A., and Fiete, I.R. (2020). Systematic errors in connectivity inferred from activity in strongly recurrent networks. Nat Neurosci 23, 1286-1296.

De La Rocha, J., Doiron, B., Shea-Brown, E., Josić, K., and Reyes, A. (2007). Correlation between neural spike trains increases with firing rate. Nature 448, 802-806.

Destexhe, A., Brette, R., and Audition, E. (2012). Springer Series in Computational Neuroscience. In Neuronal Noise (Springer).

Ding, M., Chen, Y., and Bressler, S.L. (2006). Granger Causality: Basic Theory and Application to Neuroscience. pp. q-bio/0608035.

Do, M.T.H. (2019). Melanopsin and the Intrinsically Photosensitive Retinal Ganglion Cells: Biophysics to Behavior. Neuron 104, 205-226.

Fries, P. (2005). A mechanism for cognitive dynamics: neuronal communication through neuronal coherence. Trends Cogn Sci 9, 474-480.

Fries, P. (2009). Neuronal gamma-band synchronization as a fundamental process in cortical computation. Annu Rev Neurosci 32, 209-224.

Fries, P. (2015). Rhythms for Cognition: Communication through Coherence. Neuron 88, 220-235.

Fujisawa, S., Amarasingham, A., Harrison, M.T., and Buzsaki, G. (2008). Behavior-dependent short-term assembly dynamics in the medial prefrontal cortex. Nat Neurosci 11, 823-833.

Garrett, M.E., Nauhaus, I., Marshel, J.H., and Callaway, E.M. (2014). Topography and areal organization of mouse visual cortex. J Neurosci 34, 12587-12600.

Glickfeld, L.L., and Olsen, S.R. (2017). Higher-Order Areas of the Mouse Visual Cortex. Annu Rev Vis Sci 3, 251-273.

Haider, B., Schulz, D.P., Hausser, M., and Carandini, M. (2016). Millisecond Coupling of Local Field Potentials to Synaptic Currents in the Awake Visual Cortex. Neuron 90, 35-42.

Harris, J.A., Mihalas, S., Hirokawa, K.E., Whitesell, J.D., Choi, H., Bernard, A., Bohn, P., Caldejon, S., Casal, L., Cho, A.*, et al.* (2019). Hierarchical organization of cortical and thalamic connectivity. Nature 575, 195-202.

Hasenstaub, A., Shu, Y., Haider, B., Kraushaar, U., Duque, A., and McCormick, D.A. (2005). Inhibitory postsynaptic potentials carry synchronized frequency information in active cortical networks. Neuron 47, 423-435.

Hubel, D.H., and Wiesel, T.N. (1962). Receptive fields, binocular interaction and functional architecture in the cat's visual cortex. J Physiol 160, 106-154.

Huberman, A.D., and Niell, C.M. (2011). What can mice tell us about how vision works? Trends Neurosci 34, 464-473.

Juavinett, A.L., Nauhaus, I., Garrett, M.E., Zhuang, J., and Callaway, E.M. (2017). Automated identification of mouse visual areas with intrinsic signal imaging. Nat Protoc 12, 32-43.

Jun, J.J., Steinmetz, N.A., Siegle, J.H., Denman, D.J., Bauza, M., Barbarits, B., Lee, A.K., Anastassiou, C.A., Andrei, A., Aydin, C.*, et al.* (2017). Fully integrated silicon probes for high-density recording of neural activity. Nature 551, 232-236.

Kalatsky, V.A., and Stryker, M.P. (2003). New paradigm for optical imaging: temporally encoded maps of intrinsic signal. Neuron 38, 529-545.

Kandel, E.R., Schwartz, J.H., Jessell, T.M., Biochemistry, D.o., Jessell, M.B.T., Siegelbaum, S., and Hudspeth, A. (2000). Principles of neural science, Vol 4 (McGraw-hill New York).

Koepsell, K., Wang, X., Vaingankar, V., Wei, Y., Wang, Q., Rathbun, D.L., Usrey, M.W., Hirsch, J., and Sommer, F.T. (2009). Retinal oscillations carry visual information to cortex. Frontiers in systems neuroscience 3, 4.

Kohn, A., and Smith, M.A. (2005). Stimulus dependence of neuronal correlation in primary visual cortex of the macaque. J Neurosci 25, 3661-3673.

Laboy-Juárez, K.J., Ahn, S., and Feldman, D.E. (2018). A normalized template matching method for improving spike detection in extracellular voltage recordings. bioRxiv, 445585.

Llinás, R.R. (1988). The intrinsic electrophysiological properties of mammalian neurons: insights into central nervous system function. Science 242, 1654-1664.

Magland, J., Jun, J.J., Lovero, E., Morley, A.J., Hurwitz, C.L., Buccino, A.P., Garcia, S., and Barnett, A.H. (2020). SpikeForest, reproducible web-facing ground-truth validation of automated neural spike sorters. Elife 9.

Mitzdorf, U. (1985). Current source-density method and application in cat cerebral cortex: investigation of evoked potentials and EEG phenomena. Physiological reviews 65, 37-100.

Murgas, K.A., Wilson, A.M., Michael, V., and Glickfeld, L.L. (2020). Unique Spatial Integration in Mouse Primary Visual Cortex and Higher Visual Areas. J Neurosci 40, 1862-1873.

Niell, C.M., and Stryker, M.P. (2008). Highly selective receptive fields in mouse visual cortex. J Neurosci 28, 7520-7536.

Niell, C.M., and Stryker, M.P. (2010). Modulation of visual responses by behavioral state in mouse visual cortex. Neuron 65, 472-479.

Nowak, L.G., Azouz, R., Sanchez-Vives, M.V., Gray, C.M., and McCormick, D.A. (2003). Electrophysiological classes of cat primary visual cortical neurons in vivo as revealed by quantitative analyses. Journal of neurophysiology 89, 1541-1566.

Oppenheim, A.V., and Schafer, R.W. (1975). Digital signal processing(Book). Research supported by the Massachusetts Institute of Technology, Bell Telephone Laboratories, and Guggenheim Foundation Englewood Cliffs, N J, Prentice-Hall, Inc, 1975 598 p.

Pachitariu, M., Steinmetz, N.A., Kadir, S.N., Carandini, M., and Harris, K.D. (2016a). Fast and accurate spike sorting of high-channel count probes with KiloSort. In Neural Information Processing Systems (Barcelona, Spain).

Pachitariu, M., Steinmetz, N.A., Kadir, S.N., Carandini, M., and Harris, K.D. (2016b). Fast and accurate spike sorting of high-channel count probes with KiloSort. Advances in neural information processing systems 29, 4448-4456.

Platkiewicz, J., Saccomano, Z., McKenzie, S., English, D., and Amarasingham, A. (2019). Monosynaptic inference via finely-timed spikes. p. arXiv:1909.08553.

Perkel, D.H., Gerstein, G.L., and Moore, G.P. (1967). Neuronal spike trains and stochastic point processes: II. Simultaneous spike trains. Biophysical journal 7, 419-440.

Qinglong Gu, S.L., John Murray, Richard Naud, Arvind Kumar (2020). Neuromatch Academy: Week 3, Day 1, Tutorial 1

Real Neurons: The Leaky Integrate-and-Fire (LIF) Neuron Model. (Neuromatch Academy Neuromatch).

Rossant, C., Kadir, S.N., Goodman, D.F.M., Schulman, J., Hunter, M.L.D., Saleem, A.B., Grosmark, A., Belluscio, M., Denfield, G.H., Ecker, A.S.*, et al.* (2016). Spike sorting for large, dense electrode arrays. Nat Neurosci 19, 634-641.

Saleem, A.B., Lien, A.D., Krumin, M., Haider, B., Roson, M.R., Ayaz, A., Reinhold, K., Busse, L., Carandini, M., and Harris, K.D. (2017). Subcortical Source and Modulation of the Narrowband Gamma Oscillation in Mouse Visual Cortex. Neuron 93, 315-322.

Schröder, S., Steinmetz, N.A., Krumin, M., Pachitariu, M., Rizzi, M., Lagnado, L., Harris, K.D., and Carandini, M. (2020). Arousal Modulates Retinal Output. Neuron.

Senzai, Y., Fernandez-Ruiz, A., and Buzsaki, G. (2019). Layer-Specific Physiological Features and Interlaminar Interactions in the Primary Visual Cortex of the Mouse. Neuron 101, 500-513 e505.

Sheth, S.A., Yanamadala, V., and Eskandar, E.N. (2012). Intraoperative Human Functional Brain Mapping Using Optical Intrinsic Signal Imaging. Advances in Brain Imaging, 77.

Siegle, J.H., Jia, X., Durand, S., Gale, S., Bennett, C., Graddis, N., Heller, G., Ramirez, T.K., Choi, H., Luviano, J.A.*, et al.* (2019). A survey of spiking activity reveals a functional hierarchy of mouse corticothalamic visual areas. bioRxiv, 805010.

Siegle, J.H., Pritchett, D.L., and Moore, C.I. (2014). Gamma-range synchronization of fast-spiking interneurons can enhance detection of tactile stimuli. Nat Neurosci 17, 1371-1379.

Speed, A., Del Rosario, J., Burgess, C.P., and Haider, B. (2019). Cortical State Fluctuations across Layers of V1 during Visual Spatial Perception. Cell Rep 26, 2868-2874 e2863.

Speed, A., Del Rosario, J., Mikail, N., and Haider, B. (2020). Spatial attention enhances network, cellular and subthreshold responses in mouse visual cortex. Nat Commun 11, 505.

Stark, E., and Abeles, M. (2009). Unbiased estimation of precise temporal correlations between spike trains. J Neurosci Methods 179, 90-100.

Steinmetz, N.A., Koch, C., Harris, K.D., and Carandini, M. (2018). Challenges and opportunities for large-scale electrophysiology with Neuropixels probes. Curr Opin Neurobiol 50, 92-100.

Stokes, P.A., and Purdon, P.L. (2017). A study of problems encountered in Granger causality analysis from a neuroscience perspective. Proc Natl Acad Sci U S A 114, E7063-E7072.

Storchi, R., Bedford, R.A., Martial, F.P., Allen, A.E., Wynne, J., Montemurro, M.A., Petersen, R.S., and Lucas, R.J. (2017). Modulation of Fast Narrowband Oscillations in the Mouse Retina and dLGN According to Background Light Intensity. Neuron 93, 299-307.

Tiesinga, P., and Sejnowski, T.J. (2009). Cortical enlightenment: are attentional gamma oscillations driven by ING or PING? Neuron 63, 727-732.

Trautmann, E.M., Stavisky, S.D., Lahiri, S., Ames, K.C., Kaufman, M.T., O'Shea, D.J., Vyas, S., Sun, X.L., Ryu, S.I., Ganguli, S., and Shenoy, K.V. (2019). Accurate Estimation of Neural Population Dynamics without Spike Sorting. Neuron 103, 292-+.

Vangeneugden, J., van Beest, E.H., Cohen, M.X., Lorteije, J.A.M., Mukherjee, S., Kirchberger, L., Montijn, J.S., Thamizharasu, P., Camillo, D., Levelt, C.N., *et al.* (2019). Activity in Lateral Visual Areas Contributes to Surround Suppression in Awake Mouse V1. Curr Biol 29, 4268-4275 e4267.

Vyas, S., Golub, M.D., Sussillo, D., and Shenoy, K.V. (2020). Computation Through Neural Population Dynamics. Annu Rev Neurosci 43, 249-275.

Wang, Q., Ding, S.-L., Li, Y., Royall, J., Feng, D., Lesnar, P., Graddis, N., Naeemi, M., Facer, B., and Ho, A. (2020). The Allen Mouse Brain Common Coordinate Framework: A 3D Reference Atlas. Cell.

Williams, B., Rosario, J.D., Coletta, S., Bichler, E.K., Muzzu, T., Speed, A., Meyer-Baese, L., Saleem, A.B., and Haider, B. (2020). Spatial modulation of dark versus bright stimulus responses in mouse visual cortex. bioRxiv, 2020.2010.2027.353573.

Williamson, R.C., Doiron, B., Smith, M.A., and Yu, B.M. (2019). Bridging large-scale neuronal recordings and large-scale network models using dimensionality reduction. Curr Opin Neurobiol 55, 40-47.

Wouters, J., Kloosterman, F., and Bertrand, A. (2019). SHYBRID: A graphical tool for generating hybrid ground-truth spiking data for evaluating spike sorting performance. bioRxiv, 734061.

Zhuang, J., Ng, L., Williams, D., Valley, M., Li, Y., Garrett, M., and Waters, J. (2017). An extended retinotopic map of mouse cortex. Elife 6.